Supporting Infromation

Helical Lanthanide(III) Complexes with Chiral Nonaaza Macrocycle.

Janusz Gregoliński †, Przemysław Starynowicz †, KimNgan T. Hua ‡, Jamie L. Lunkley ‡, Gilles Muller ‡ and Jerzy Lisowski**

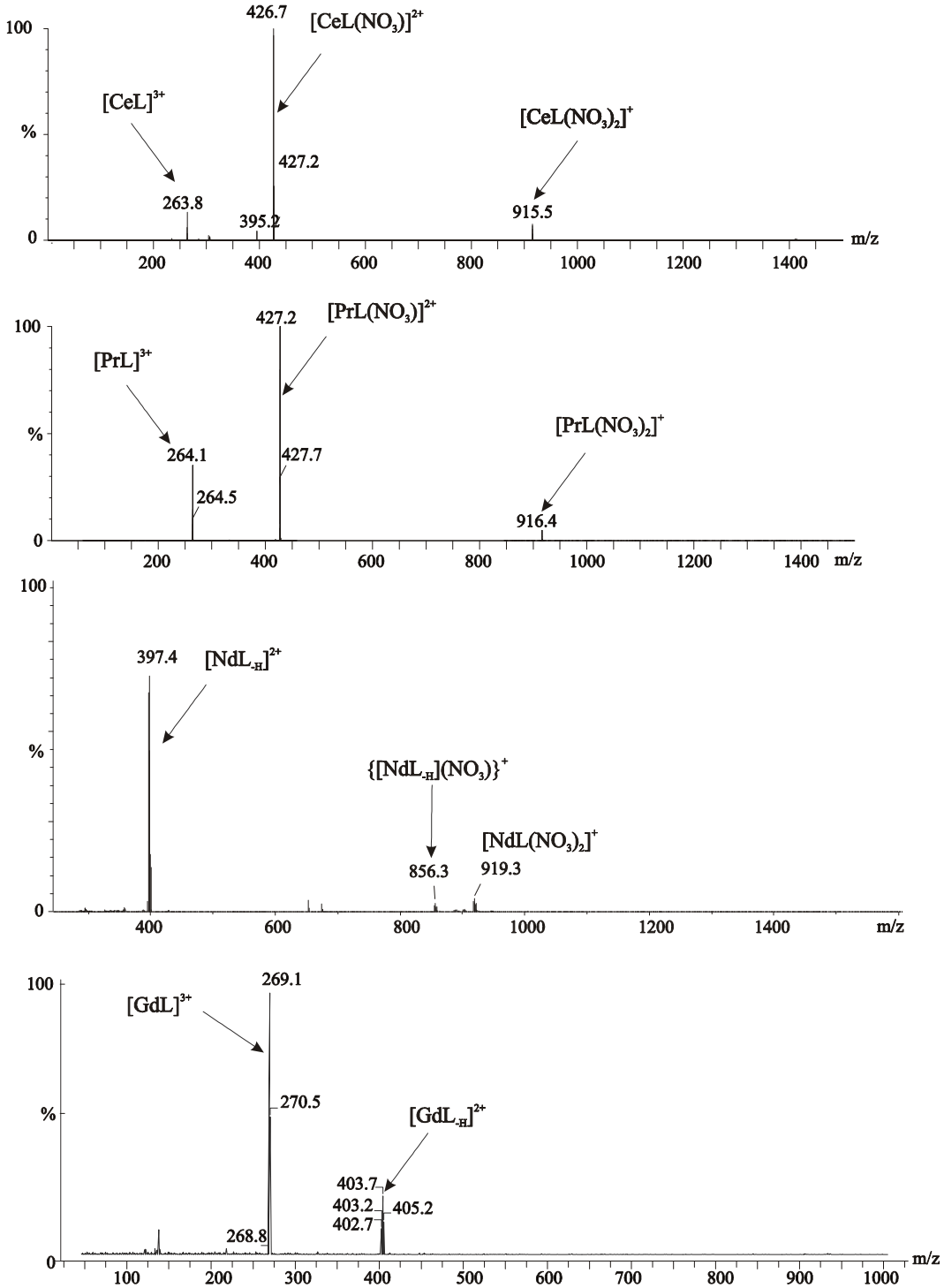

Fig. S1. ESI MS spectra of 10^{-6} M methanol solutions of the *(M)*-[Ce$\mathbf{L}_{RRRRRR}$]$(NO_3)_3$•$2H_2O$, *(M)*-[Pr$\mathbf{L}_{RRRRRR}$]$(NO_3)_3$•H_2O, [Nd$\mathbf{L}_{RRRRRR}$]$(NO_3)_3$•$0.5H_2O$ and *(M)*-[Gd$\mathbf{L}_{RRRRRR}$]$(NO_3)_3$•$4H_2O$ complexes.

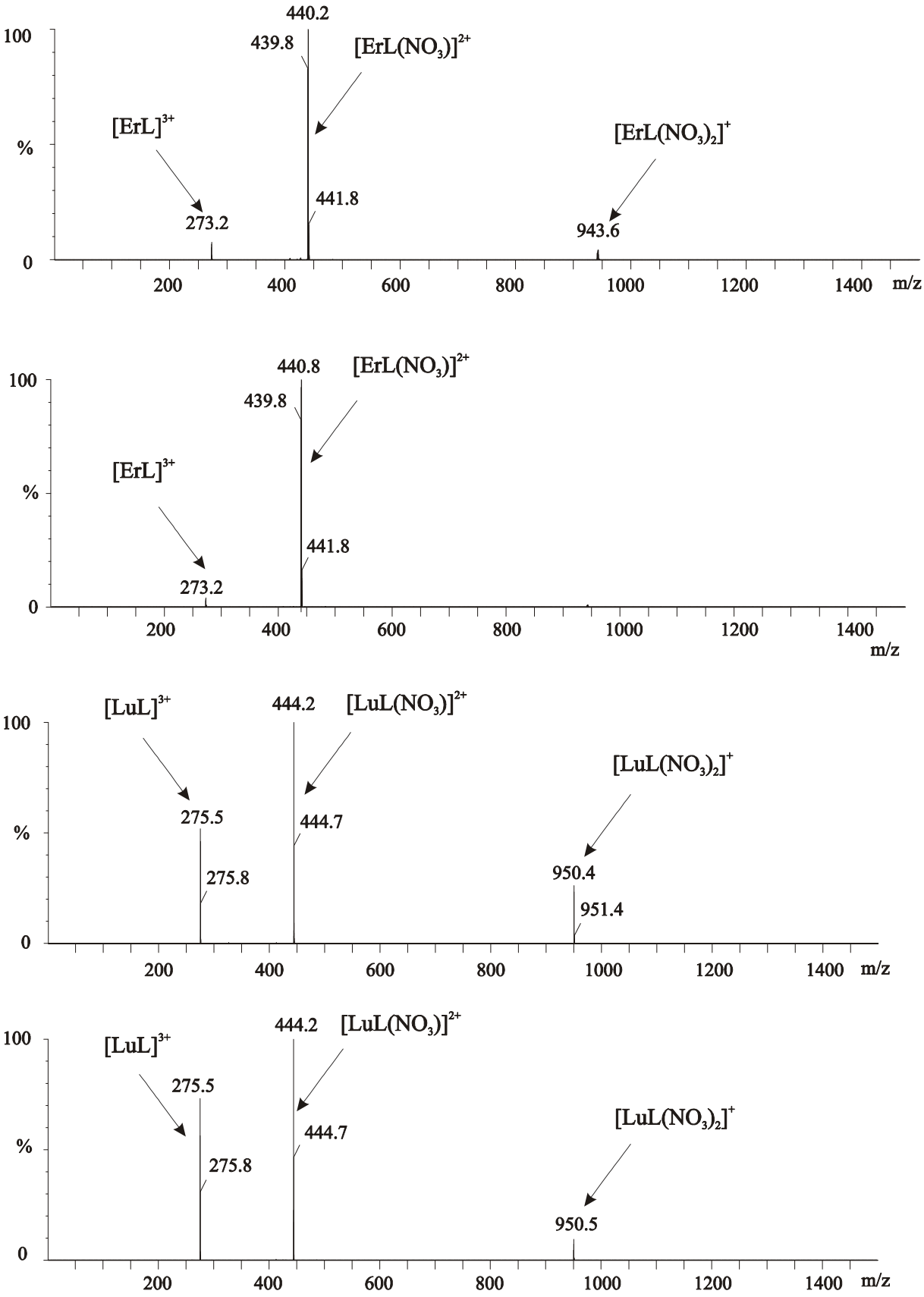

Fig. S2. ESI MS spectra of 10^{-6} M methanol solutions of the (*M*)-[Er$\mathbf{L}_{RRRRRR}$]$(NO_3)_3$•$CHCl_3$•$2.5H_2O$, (*P*)-[Er$\mathbf{L}_{RRRRRR}$]$(NO_3)_3$•$7H_2O$, (*M*)-[Lu$\mathbf{L}_{RRRRRR}$]$(NO_3)_3$•$CHCl_3$•$2H_2O$ and (*P*)-[Lu$\mathbf{L}_{RRRRRR}$]$(NO_3)_3$•$7H_2O$ complexes.

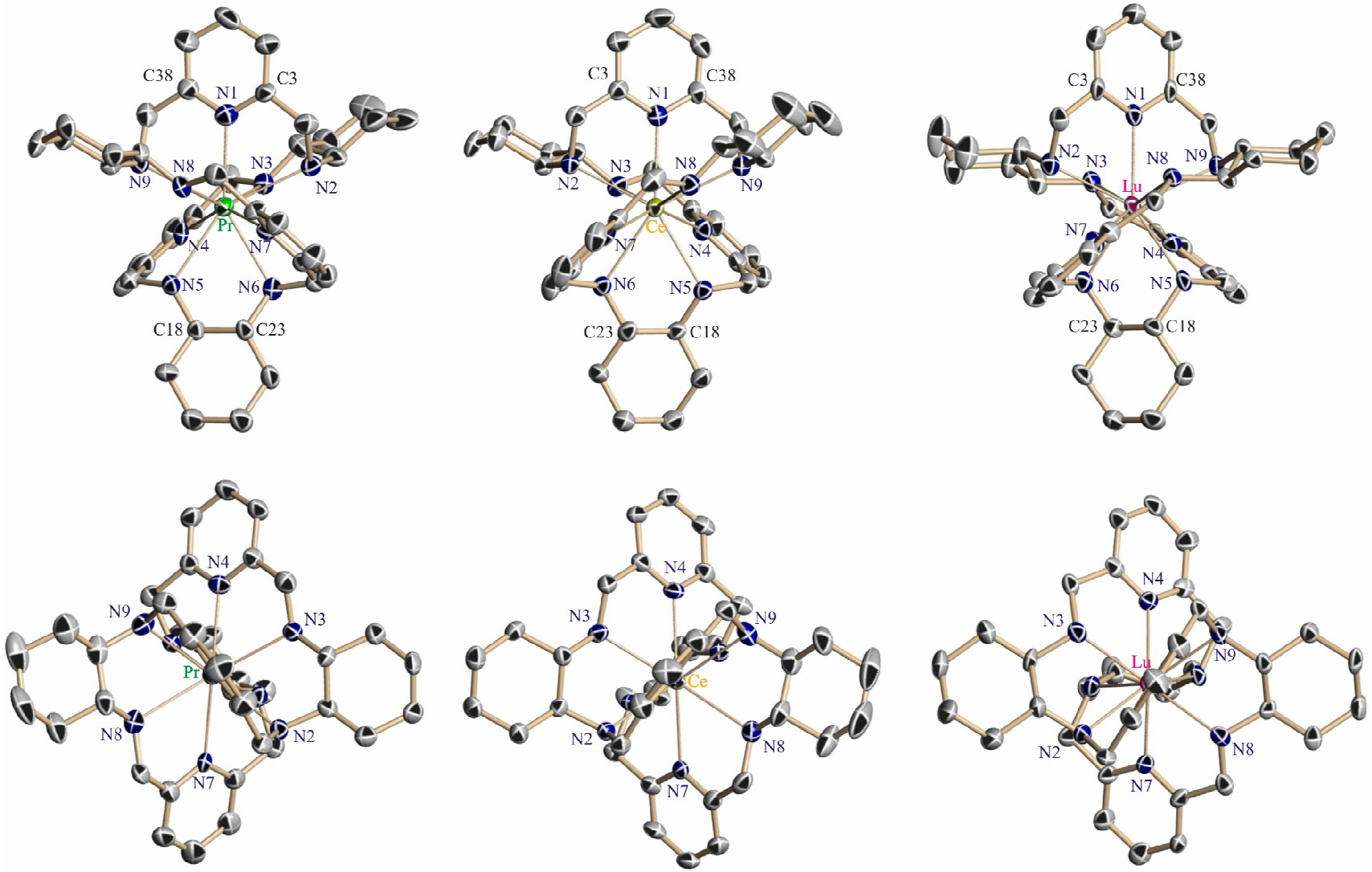

Fig. S3. Views of the structure of the *(M)*-[Pr**L**$_{RRRRRR}$]$^{3+}$ (left), *(P)*-[Ce**L**$_{SSSSSS}$]$^{3+}$ (middle) and *(P)*-[Lu**L**$_{RRRRRR}$]$^{3+}$ cations along (upper pictures) and perpendicular to the C_2 axis (lower pictures).

Description of X-ray crystal structures

The crystals of (*M*)-[Pr**L**$_{RRRRRR}$]$(NO_3)_3$•$3CH_3CN$•$3^2/_3H_2O$, (*P*)-[Ce**L**$_{SSSSSS}$]$(NO_3)_3$•$4CH_3CN$•$3H_2O$ and (*P*)-[Lu**L**$_{RRRRRR}$]$(NO_3)_3$•$1^7/_8CH_3CN$•$3^3/_4H_2O$ are composed of the complex cation $[Ln\mathbf{L}]^{3+}$, uncoordinated nitrate anions, and partially disordered solvent molecules (Supporting Table S1). In each complex the cation is surrounded by all nine nitrogen atoms of the ligand and is not coordinated by the solvent molecules or counteranions

The **Type I** and **Type II** diastereomers differ in the configuration at the amine nitrogen atoms. In **Type I** complexes, the helical twist of the macrocycle imposes the *S*, *S* chirality[18] of the nitrogen atoms of the unique cyclohexane ring and *R*, *S* chirality of the nitrogen atoms of the two equivalent cyclohexane rings. In **Type II** complexes, the opposite helix direction imposes also different chirality at the donor nitrogen atoms; the nitrogen atoms of the unique cyclohexane ring positioned on the symmetry axis are of *R* configuration, while the remaining four amine nitrogen atoms are of *S* configuration.

The three 2,6-substituted pyridine fragments of the macrocycle **L** in the (*P*)-[Lu**L**$_{RRRRRR}$]$^{3+}$ complex form propeller-like structure (Fig. S4), similar to that observed in tris(dipicolinato)lanthanide anions[19] or some pyridine-containing triple-helical[8] lanthanide(III) complexes. Similarly to the tris(dipicolinato)lanthanide anions, the coordination figure of the metal cation may be viewed as a distorted tricapped trigonal prism (TCTP) with twisted bases, where the amine atoms N2, N3, N6 and N5, N8, N9 span the bases, and the pyridine atoms N1, N4, N7 form the caps. The further distortion of the coordination sphere results from the fact that the D_3 symmetry is not observed and only one two-fold symmetry axis of the parent idealized tricapped trigonal prism structure is retained. Similar propeller-like arrangement of pyridine fragments is also observed for the (*P*)-[Ce**L**$_{SSSSSS}$]$^{3+}$ and (*M*)-

[Pr$\mathbf{L}_{RRRRRR}$]$^{3+}$ cations (Fig. S5), but the deviations from the D_3 symmetry and tricapped trigonal prism structure are even greater.

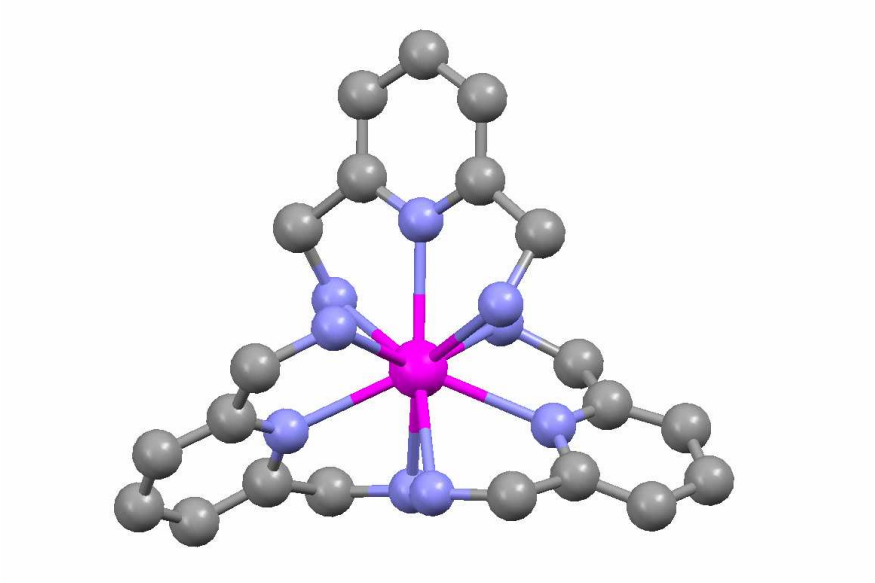

Fig. S4. The propeller-like arrangement of the pyridine fragments in the (*P*)-[Lu$\mathbf{L}_{RRRRRR}$]$^{3+}$ complex (cyclohexane rings of the $\mathbf{L}_{RRRRRR}$ macrocycle are not shown for clarity)

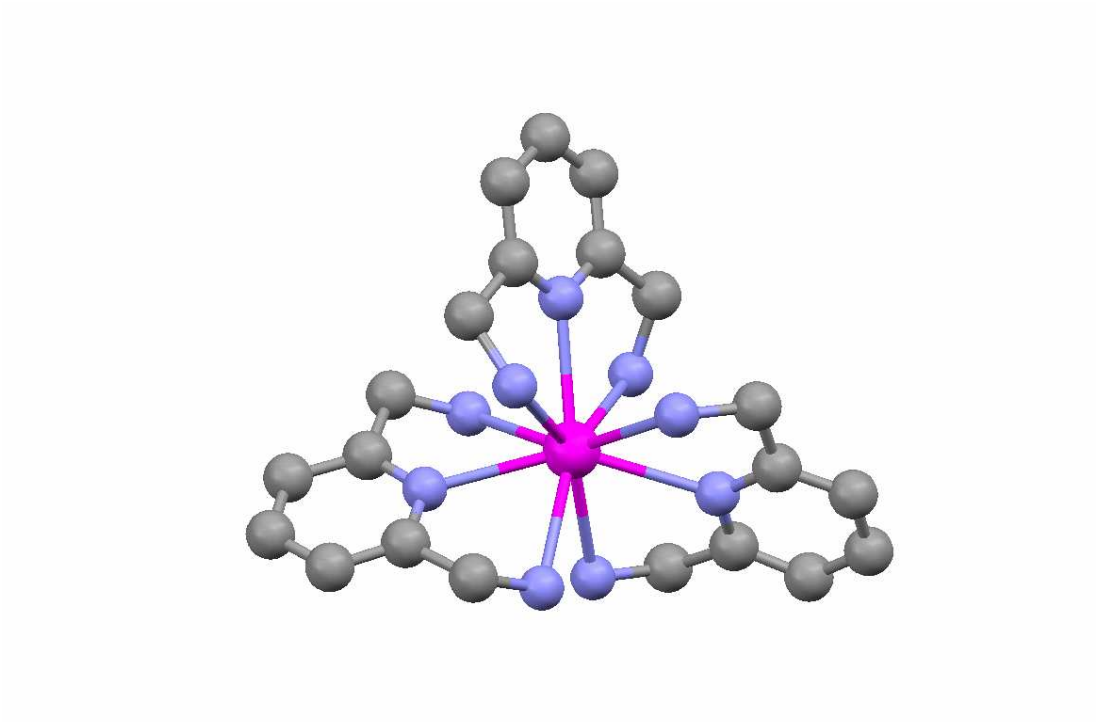

Fig. S5. The propeller-like arrangement of the pyridine fragments in the (M)-[PrL_{RRRRRR}]$^{3+}$ complex (cyclohexane rings of the L_{RRRRRR} macrocycle are not shown for clarity)

Additionally, the crystals of the approximate composition (*M*)-[Ce$\mathbf{L}_{RRRRRR}$][Ce$(NO_3)_x(H_2O)_y$]$(NO_3)_{(6-x)}$•solv. (orthorhombic $C222_1$, a = 15.116(1), b = 19.985(1), c = 34.153(2)) were obtained by slow diffusion of diethyl ether into the CH_3OH/CH_3CN solution of the (*M*)-[Ce$\mathbf{L}_{RRRRRR}$]$(NO_3)_3$•$2H_2O$ complex, whereas the crystals of the approximate composition (*M*)-[Pr$\mathbf{L}_{RRRRRR}$][Pr$(NO_3)_x(H_2O)_n$]$(NO_3)_{(5-x)}$Cl•solv. (orthorhombic $C222_1$, a = 15.171(4), b = 19.956(5), c = 33.79(10)) were obtained by the slow evaporation of the solution containing the (*M*)-[Pr$\mathbf{L}_{RRRRRR}$]$(NO_3)_3$•H_2O complex in chloroform/methanol mixture. Although the solvent and counteranion molecules were severely disordered and crystals were too small to obtain satisfactory solved molecular structures, the model structures obtained definitely show the *M*-helical conformation of the ligand in both complexes (Fig. S6). For similar reasons, the structure of the crystals of the composition *(P)*-[Yb$\mathbf{L}_{RRRRRR}$][$Yb_{0.5}(NO_3)_{1.5}(H_2O)_{1.5}$]$(NO_3)_3$•$2.75H_2O$ (trigonal $P322_1$, a=15.486(2), c = 38.307(8)), obtained after one month from the methanol/acetonitrile solution of the (*M*)-[Yb$\mathbf{L}_{RRRRRR}$]$_2$[Yb$(NO_3)_5$]$(NO_3)_4$•$4H_2O$ complex, was not satisfactorily solved. However, the model structure clearly showed the (*P*)-helical conformation of the conversion product of the starting (*M*)-helical complex (Fig. S7).

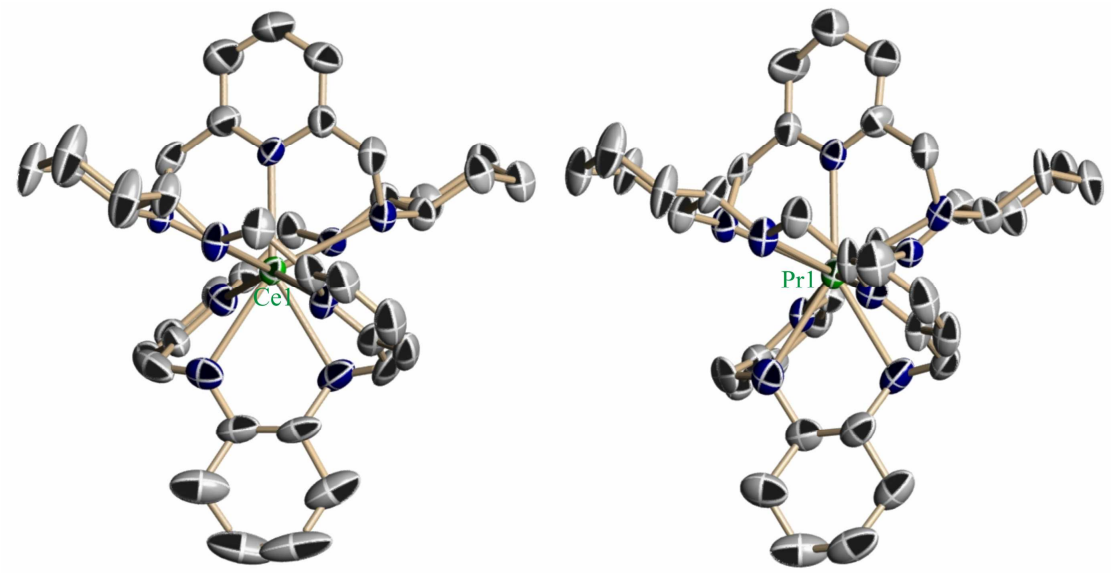

Fig. S6. The model structures of the cationic complexes: (*M*)-[Ce$\mathbf{L}_{RRRRRR}$]$^{3+}$ (left) and (*M*)-[Pr$\mathbf{L}_{RRRRRR}$]$^{3+}$ (right) in highly disordered (*M*)-[Ce$\mathbf{L}_{RRRRRR}$][Ce$(NO_3)_x(H_2O)_y$]$(NO_3)_{(6-x)}$•solv. and (*M*)-[Ln$\mathbf{L}_{RRRRRR}$][Ln$(NO_3)_x(H_2O)_n$]$(NO_3)_{(5-x)}$Cl•solv. crystals.

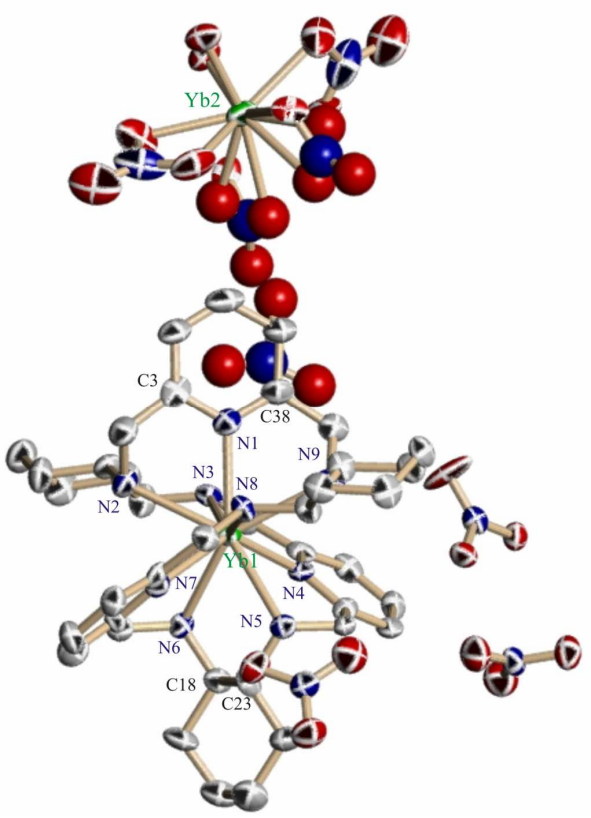

Fig. **S7.** Model structure of *(P)*-[Yb$\mathbf{L}_{RRRRRR}$][$Yb_{0.5}(NO_3)_{1.5}(H_2O)_{1.5}$]$(NO_3)_3$•2.75$H_2O$.

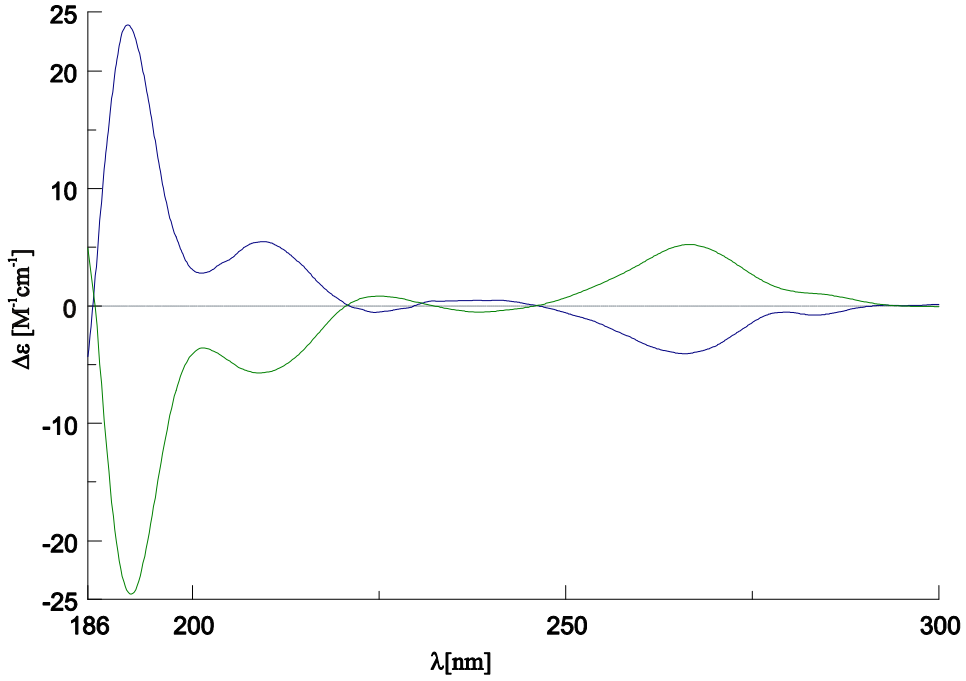

Fig. S8. The CD spectra of the two enantiomeric [Pr**L**](NO$_3$)$_3$•H$_2$O complexes in H$_2$O solutions (1 × 10^{-3} M): (*M*)-[Pr$\mathbf{L}_{RRRRRR}$]$^{3+}$ (green)/ (*P*)-[Pr$\mathbf{L}_{SSSSSS}$]$^{3+}$ (blue).

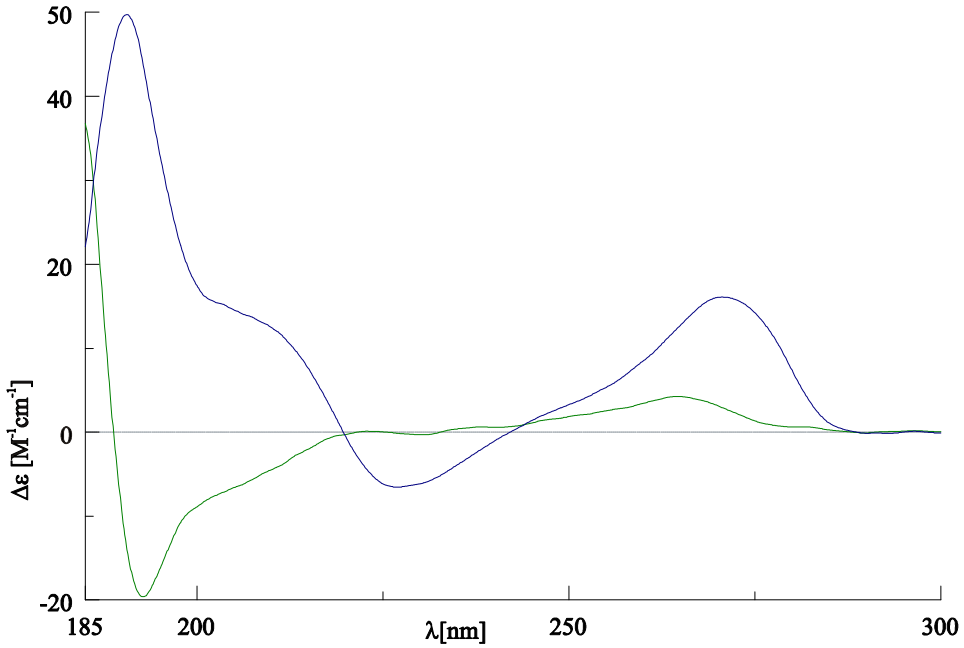

Fig. S9. The CD spectra of the two diastereomers of the Lu(III) complexes with $\mathbf{L}_{RRRRRR}$ in H$_2$O solutions (1 × 10^{-3} M): (*M*)-[Lu$\mathbf{L}_{RRRRRR}$]$^{3+}$ (green) / (*P*)-[Lu$\mathbf{L}_{RRRRRR}$]$^{3+}$ (blue). The spectra were recorded at RT during 20 minutes after both complexes had been dissolved. The solution of the (*M*)-[Ln$\mathbf{L}_{RRRRRR}$]$^{3+}$ isomer includes ca 5% of free ligand $\mathbf{L}_{RRRRRR}$ (based on ^{1}H NMR spectrum carried out during the same time).

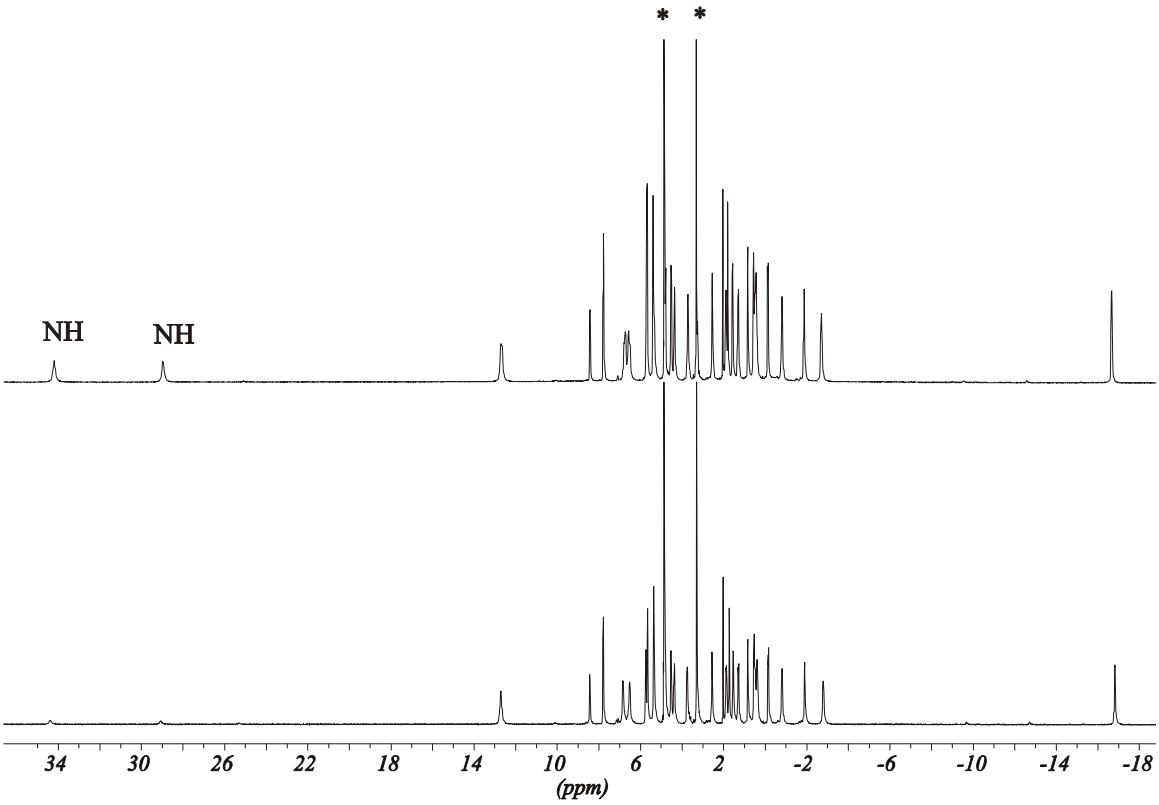

Fig. **S10**. ^{1}H NMR spectra of *(M)*-[Eu$\mathbf{L}_{RRRRRR}$]$(NO_3)_3$•$4H_2O$ in CD_3OD solution (1×10^{-2} M) immediately after being dissolved (upper trace) and after 3 days (lower trace). (* - residual solvent signals)

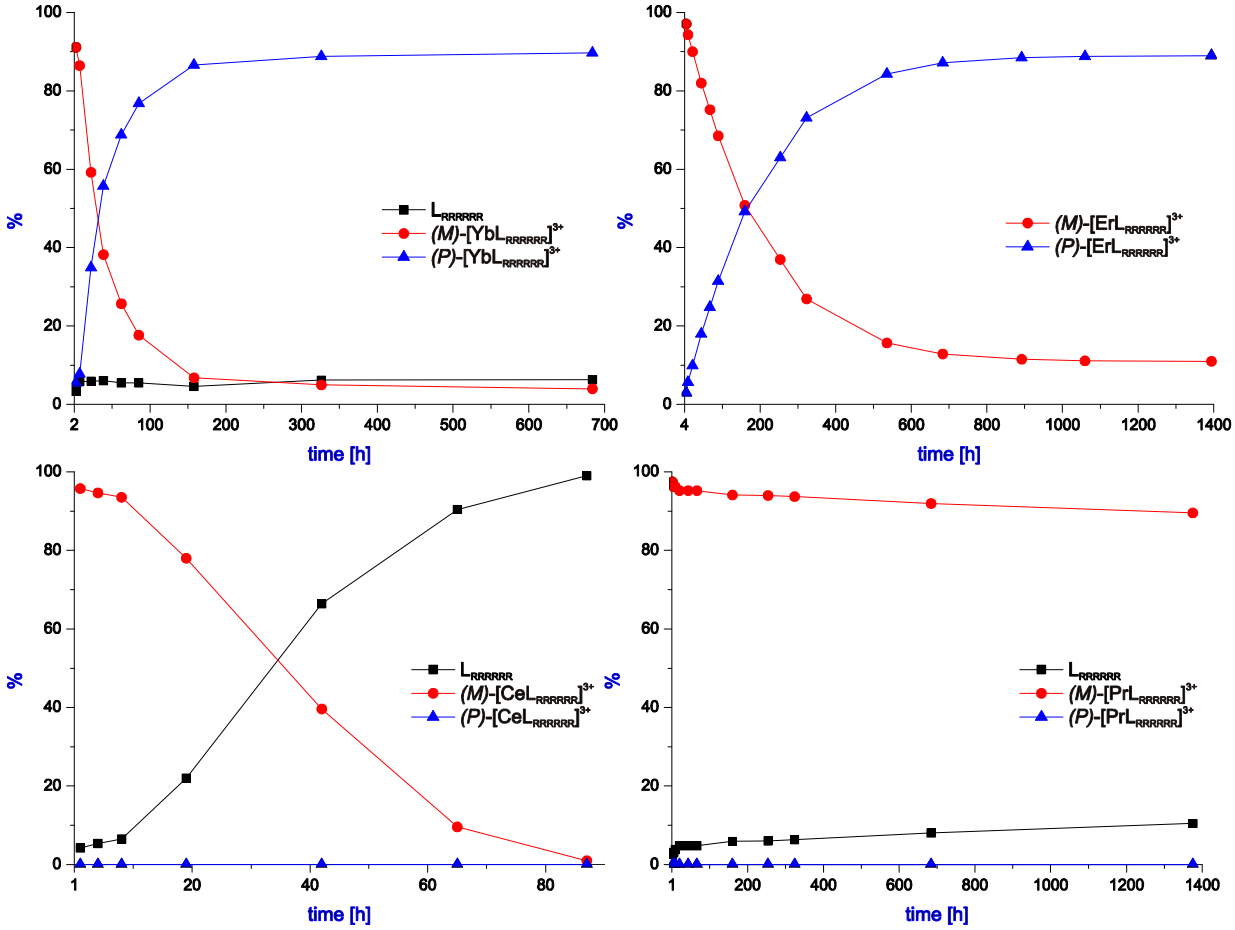

Fig. S11. The dependence of the relative concentration of the (*M*)- and (*P*)-diastereomers on the heating time of the 1 × 10^{-2} M solution of (*M*)-[Ln**L**$_{RRRRRR}$]$(NO_3)_3$] (D_2O, 318 K). The red, blue and black plots represent the (*M*)-, (*P*)-[Ln**L**$_{RRRRRR}$]$^{3+}$ complexes, and the free ligand **L**$_{RRRRRR}$, respectively.

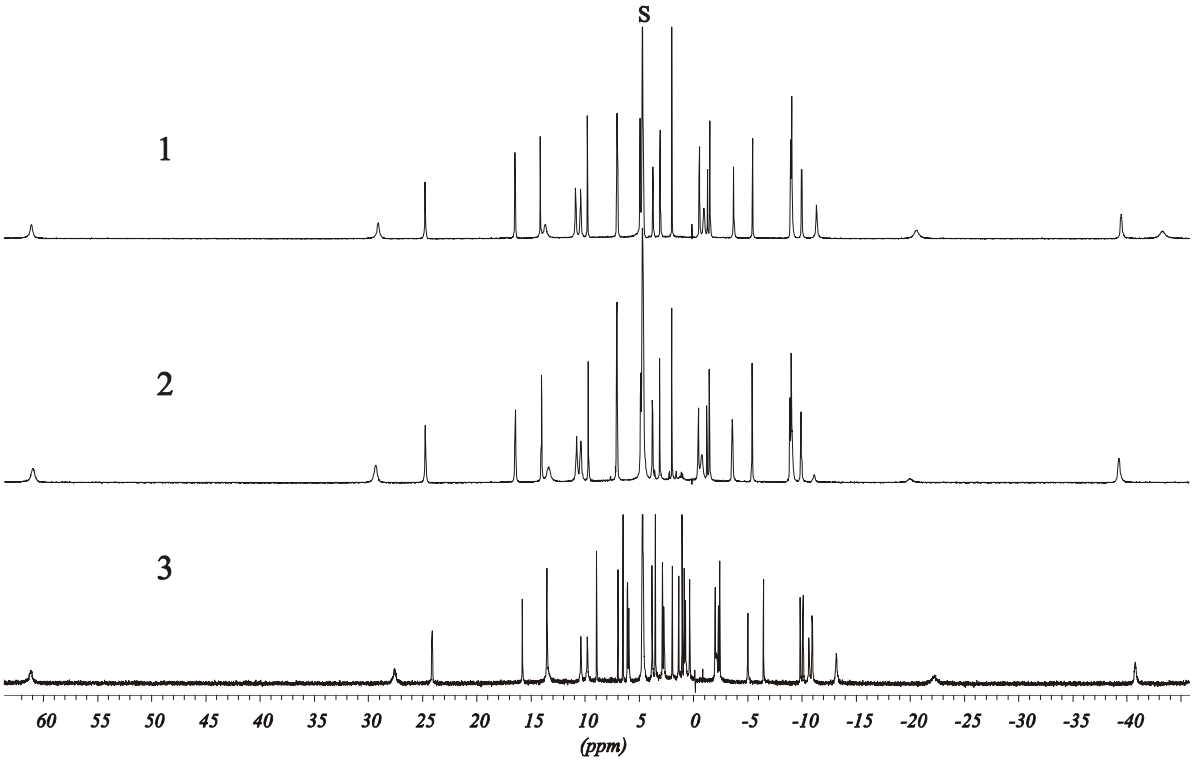

Fig. **S12.** ^{1}H NMR spectra of *(P)*-[Yb$\mathbf{L}_{RRRRRR}$]$(NO_3)_3$•6H_2O (1 × 10^{-2} M) in D_2O solution (1), in D_2O solution in the presence of 3 equivalents of NaOH (2), in 20% DCl solution measured after 17 days (3). (S – solvent signal)

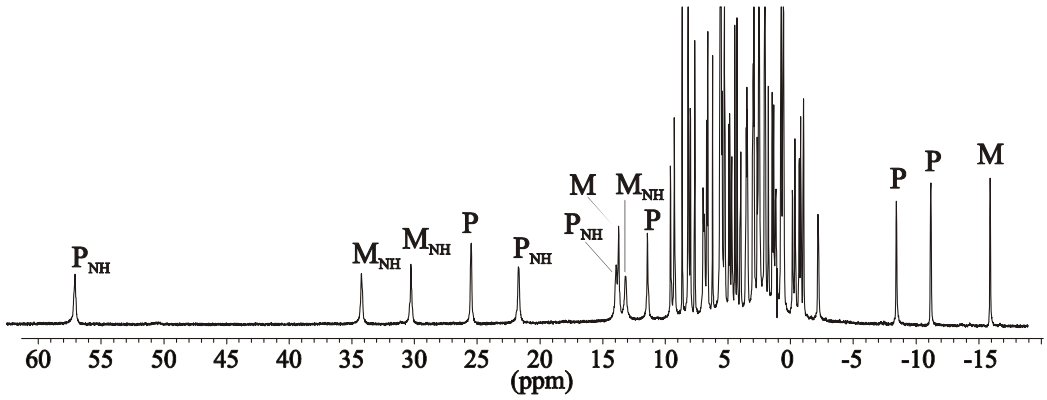

Fig. S13. The ^{1}H NMR spectrum of the mixture of Eu(III) complexes enriched in the (*P*)-diastereomer with a (*M*)-[Eu**L**$_{RRRRRR}$]$^{3+}$/(*P*)-[Eu**L**$_{RRRRRR}$]$^{3+}$ ratio equal to 1:1 (the 1×10^{-2} M D_2O solution, 298 K)

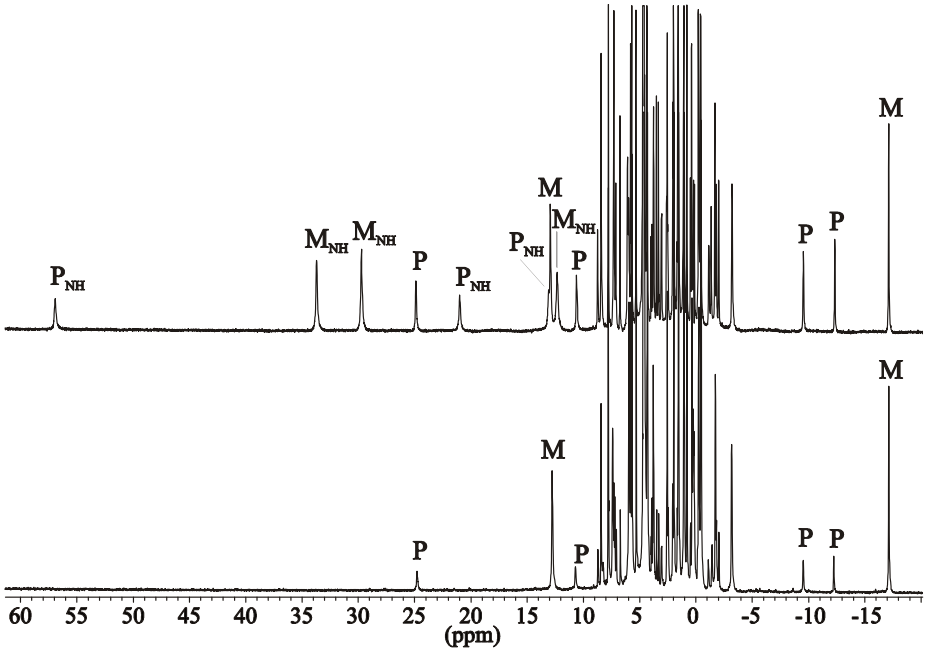

Fig S14. Upper trace -the ^{1}H NMR spectrum of the mixture of Eu(III) complexes enriched in the *(P)*-diastereomer with a (*M*)-[Eu**L**$_{RRRRRR}$]$^{3+}$/(*P*)-[Eu**L**$_{RRRRRR}$]$^{3+}$ ratio equal to 2:1. Lower trace – the ^{1}H NMR of the same sample measured after 20 days. (1×10^{-2} M D_2O solution, 298 K)

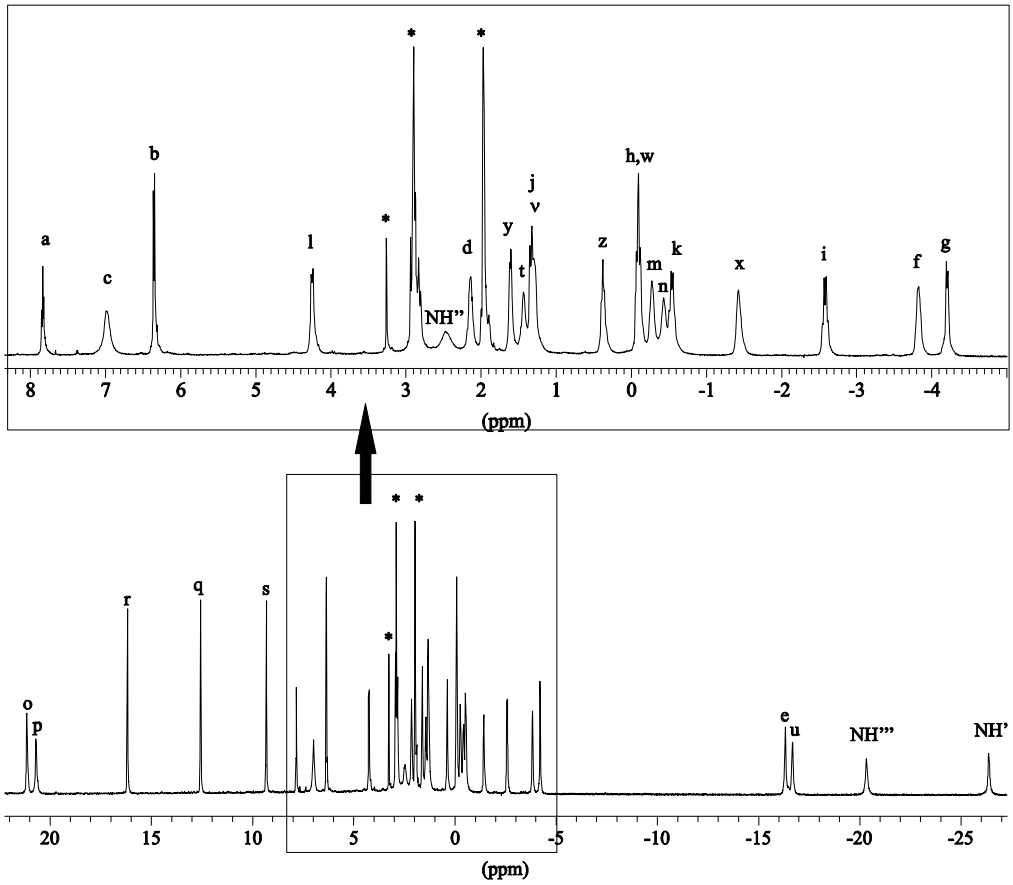

Supporting Fig S15. The ^{1}H NMR spectrum of the *(M)*-[Pr**L**$_{RRRRRR}$]$(NO_3)_3$•H_2O complex in CD_3CN/CD_3OD 8:1 v/v solution (298K). See Scheme 1 for the labeling of the positions.

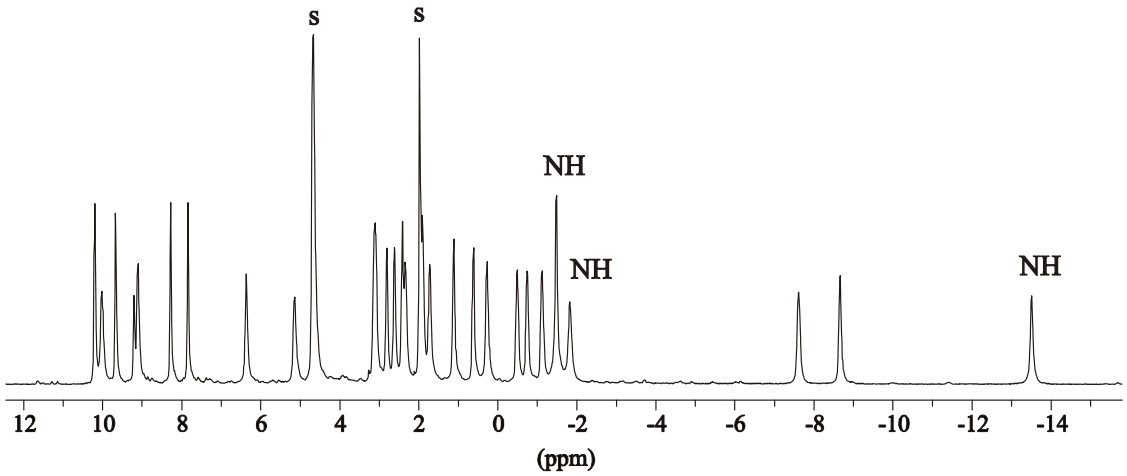

Fig. S16. The ^{1}H NMR spectrum of the (*M*)-[Ce$\mathbf{L}_{RRRRRR}$]$(NO_3)_3$•$2H_2O$ complex in D_2O solution (1×10^{-2} M, 298 K)

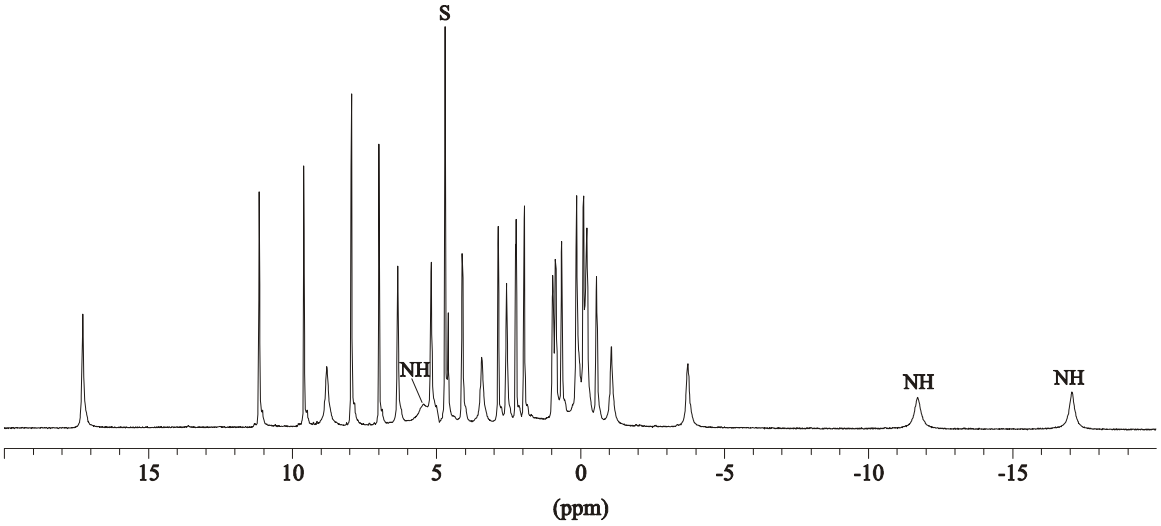

Fig. S17. ^{1}H NMR spectrum of the(*M*)-[Nd$\mathbf{L}_{SSSSSS}$]$(NO_3)_3$•$0.5H_2O$ complex in D_2O solution (1×10^{-2} M, 298 K).

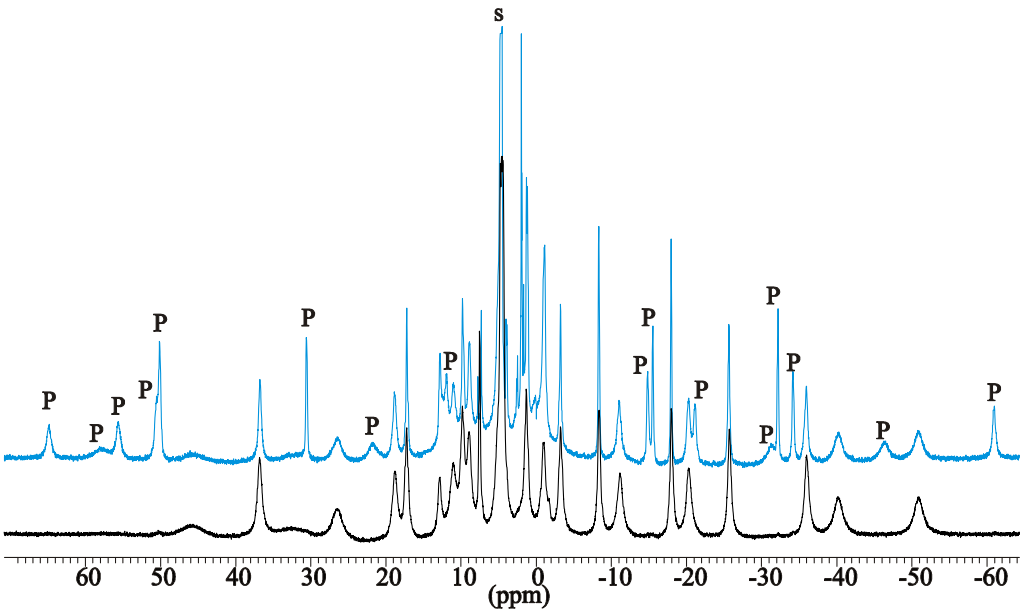

Fig S18. ^{1}H NMR spectra of the (*M*)-[Tb**L**$_{RRRRRR}$](NO$_3$)$_3$•4H$_2$O complex (black trace) and of the sample enriched in the (*P*)-isomer with a (*M*)-[Tb**L**$_{RRRRRR}$]$^{3+}$/(*P*)-[Tb**L**$_{RRRRRR}$]$^{3+}$ ratio equals to 10:8 in D$_2$O solutions (1 × 10^{-2} M, 298 K).

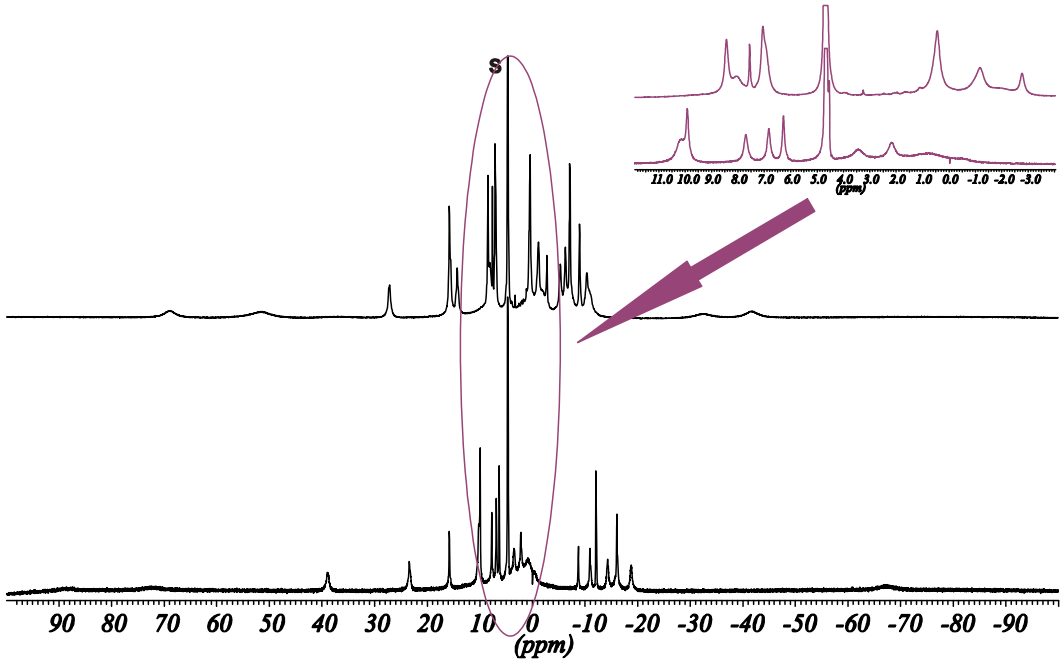

Fig. S19. ^{1}H NMR spectra of the (*M*)-[Er**L**$_{RRRRRR}$](NO$_3$)$_3$•CHCl$_3$•2.5H$_2$O (upper trace) and (*P*)-[Er**L**$_{RRRRRR}$](NO$_3$)$_3$•7H$_2$O complexes (lower trace) in D$_2$O solutions (1 × 10^{-2} M, 298 K).

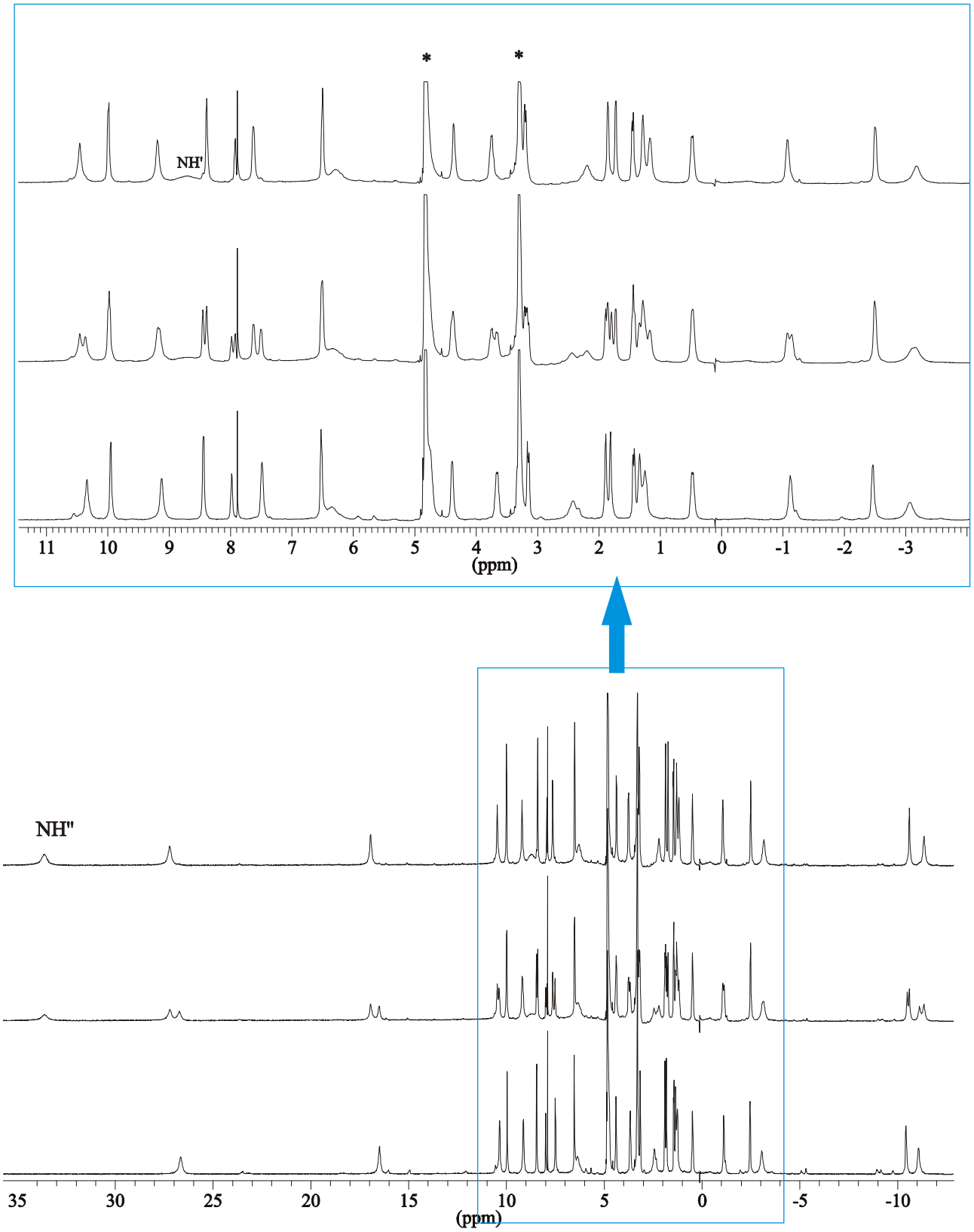

Fig. **S20**. The NMR spectra of (*M*)-[Yb**L**$_{RRRRRR}$]$(NO_3)_3$•$CHCl_3$•H_2O complex in CD_3OD solution (298 K), illustrating the doubling of the resonances due to isotope effect. The spectra were measured 10 min. (top), 3 hrs (middle) and 22 hrs (bottom) after preparation of the sample.

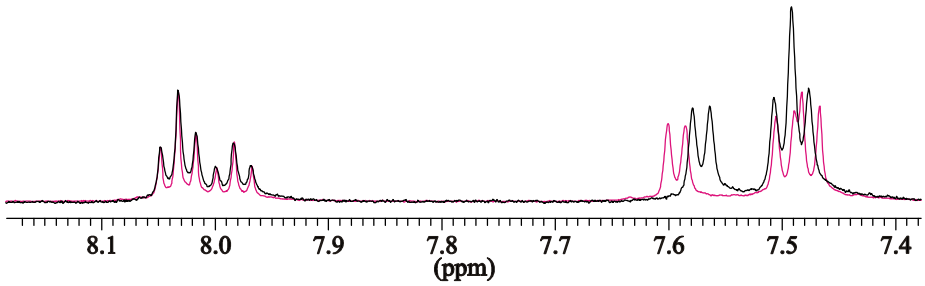

Fig. S21. Fragments of the ^{1}H NMR spectra of the (*M*)-[Lu**L**$_{RRRRRR}$](NO$_3$)$_3$•CHCl$_3$•2H$_2$O (black trace) and (*P*)-[Lu**L**$_{RRRRRR}$](NO$_3$)$_3$•7H$_2$O (red trace) in D$_2$O solutions (1×10^{-2} M, 298 K).

^{1}H NMR signal assignment

Because some of the 2D NMR correlations were difficult to observe due to paramagnetic relaxation in the case of Pr(III) complex and partial signal overlap in the case of Lu(III) complex, only the combined results obtained from COSY, TOCSY, NOESY, ROESY and HMQC spectra allowed unequivocal assignment of all resonances.

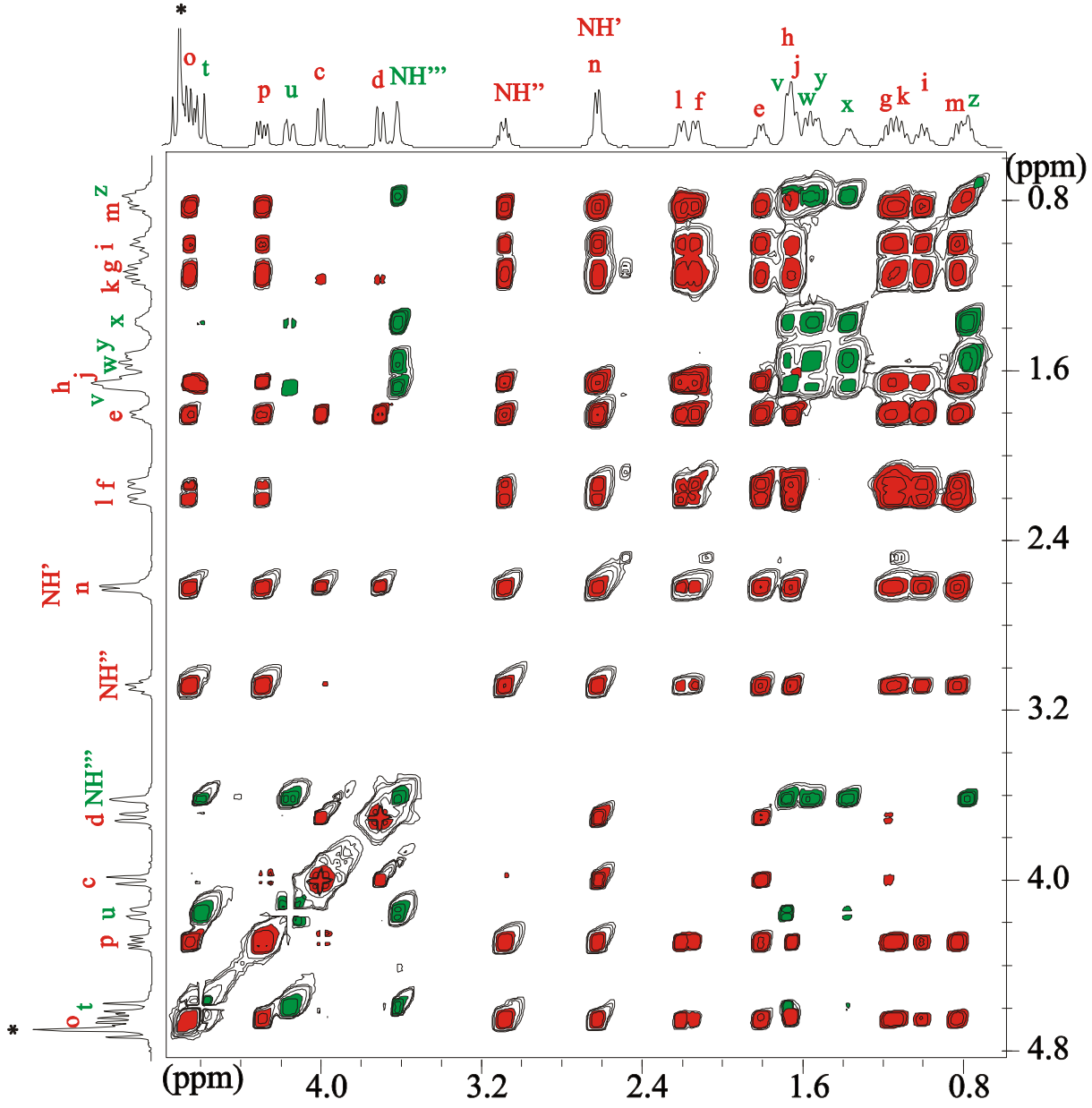

Fig. S22. The TOCSY spectrum of the (*P*)-[Lu**L**$_{RRRRRR}$](NO$_3$)$_3$•7H$_2$O complex (D$_2$O, 298K). The red and green colors indicate the spin systems **e+f+g+h+i+j+k+l+m+n+c+d+NH'+NH''+o+p** and **v+w+x+y+z+t+u+NH'''**, respectively. See Scheme 1 for the labeling of the positions.

The TOCSY spectrum of the D_2O solution of (*P*)-[Lu**L**$_{RRRRRR}$]$(NO_3)_3$ complex identifies a group of 16 correlated signals and a group of 8 correlated signals (Fig. S22). These two spin systems correspond to two sets of cyclohexane protons: **e**+**f**+**g**+**h**+**i**+**j**+**k**+**l**+**m**+**n** and **v**+**w**+**x**+**y**+**z**, respectively, together with the adjacent NH and methylene bridge protons: **c**+**d**+**NH'**+**NH''**+**o**+**p** and **t**+**u**+**NH'''**, respectively (see Scheme 1 for labelling). The HMQC spectrum identifies the ^{1}H NMR signals of pairs of geminal protons and confirms the assignment of the group of the 3 signals of the exchangeable NH protons (Supporting Fig. S23). This spectrum also allows finding the signals of cyclohexane C*H*NH protons that do not have a geminal partner, i.e. signal **v** from the above group of eight TOCSY-correlate signals and the pair of signals **e**+**n** from the above group of sixteen TOCSY-correlate signals. The identification of the **e**+**n** pair is additionally confirmed by observation of the COSY correlation (Supporting Fig. S24) between these two signals.

The assignment of signals starts with the easily assigned signal of pyridine proton **a** (Scheme 1), positioned on the symmetry axis, that integrates to 1H, while all other signals integrate to 2H. Signal **a** is ROESY (Fig. 5), NOESY and COSY (Supporting Fig. S24) correlated to a signal of aromatic proton **b**. The signal of the proton **b** is in turn ROESY correlated to the signals of the pair of geminal protons **c** and **d**, and signal of proton **e**. Signals of protons **e** and **c** are also ROESY correlated. The assignment of signal **e** allows for finding of the signal of the proton **n**, since the pair **e**+**n** has been already identified. Signal of proton **n** is ROESY correlated to the signals of the pair of geminal protons **o** and **p**, and ROESY and COSY correlated to the signal of amine proton **NH''**. Similarly, the signals of methylene bridge protons **c** and **d** are COSY correlated to signal of amine proton **NH'** (overlapped with signal of proton **n**). Thus the remaining COSY correlated signals of methylene bridge and amine proton correspond to positions **t**, **u** and **NH'''**, respectively. The signals of geminal protons **o** and **p** are ROESY correlated to signal of aromatic proton **q**, similarly the signals of geminal protons **t** and **u** are ROESY correlated to the signal of aromatic proton **s**. The analysis of the remaining COSY and NOESY/ROESY correlations within the cyclohexane rings

allows assignment of the remaining signals (Supporting Fig. S25). The HMQC spectrum in combination with the assignment of ^{1}H NMR signals enables also the assignment of ^{13}C NMR signals of the corresponding carbon atoms (Supporting Fig. S23). Similar analysis was also performed for the 2D NMR spectra of the DMSO-d6 solution of the Lu(III) complex and the CD_3CN/CD_3OD solution of the Pr complex (Fig. S15).

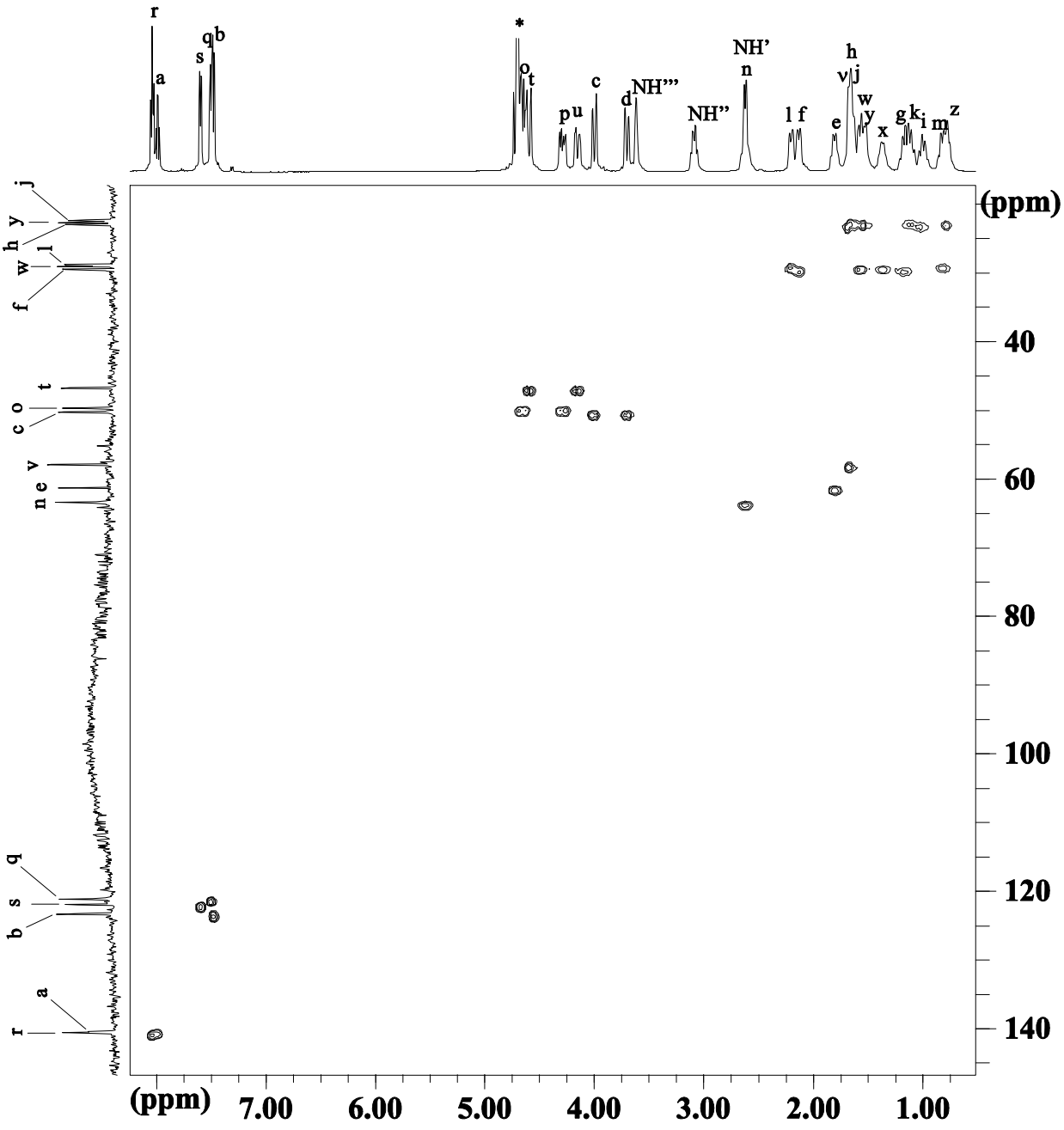

Fig. S23. HMQC spectrum of the (*P*)-[Lu**L**$_{RRRRRR}$]$(NO_3)_3$•$7H_2O$ complex in D_2O solution (1×10^{-2} M, 298 K)

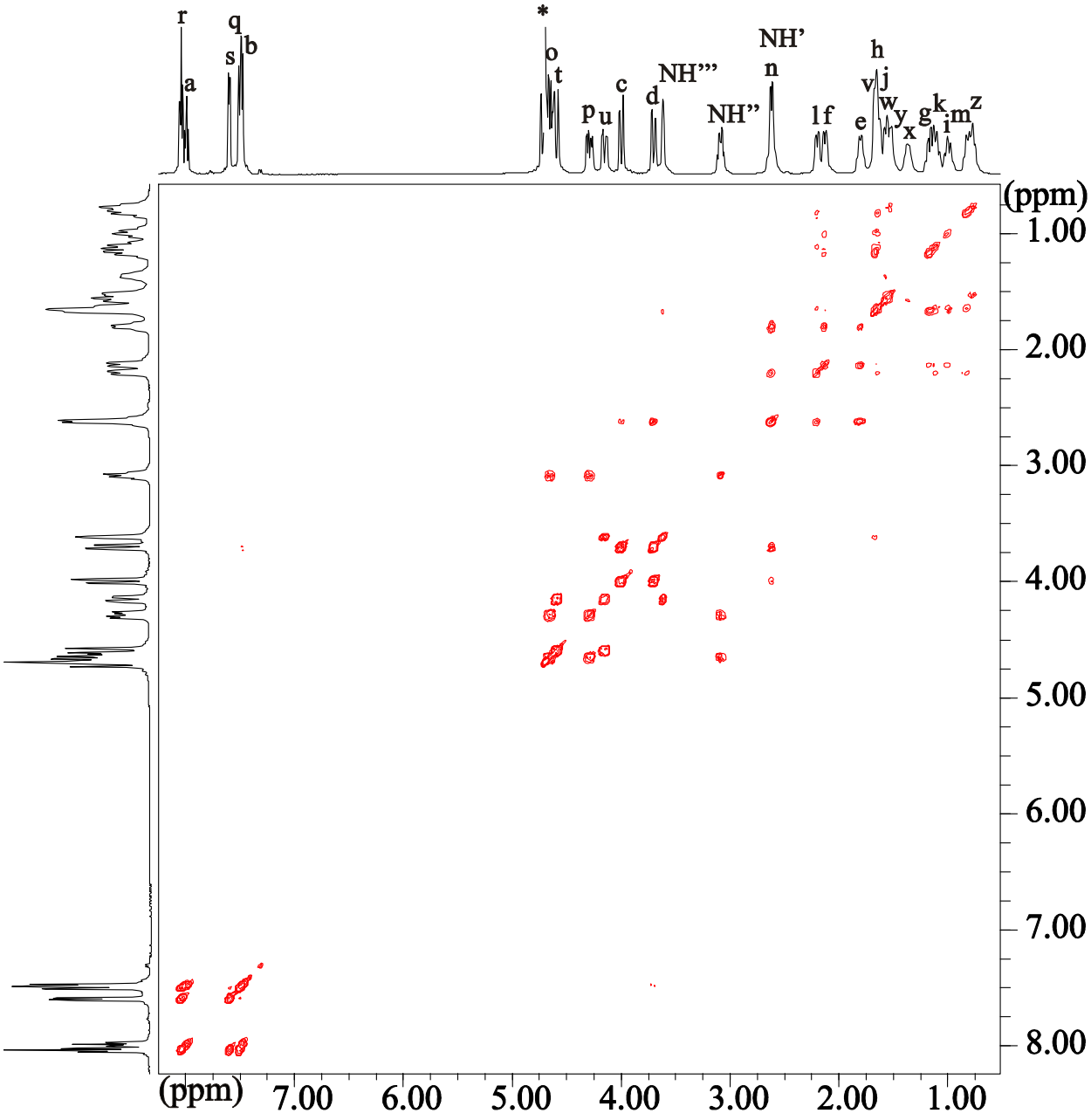

Fig. S24. COSY spectrum of the (*P*)-[Lu**L**$_{RRRRRR}$](NO$_3$)$_3$•7H$_2$O complex in D$_2$O solution (1 × 10^{-2} M, 298 K)

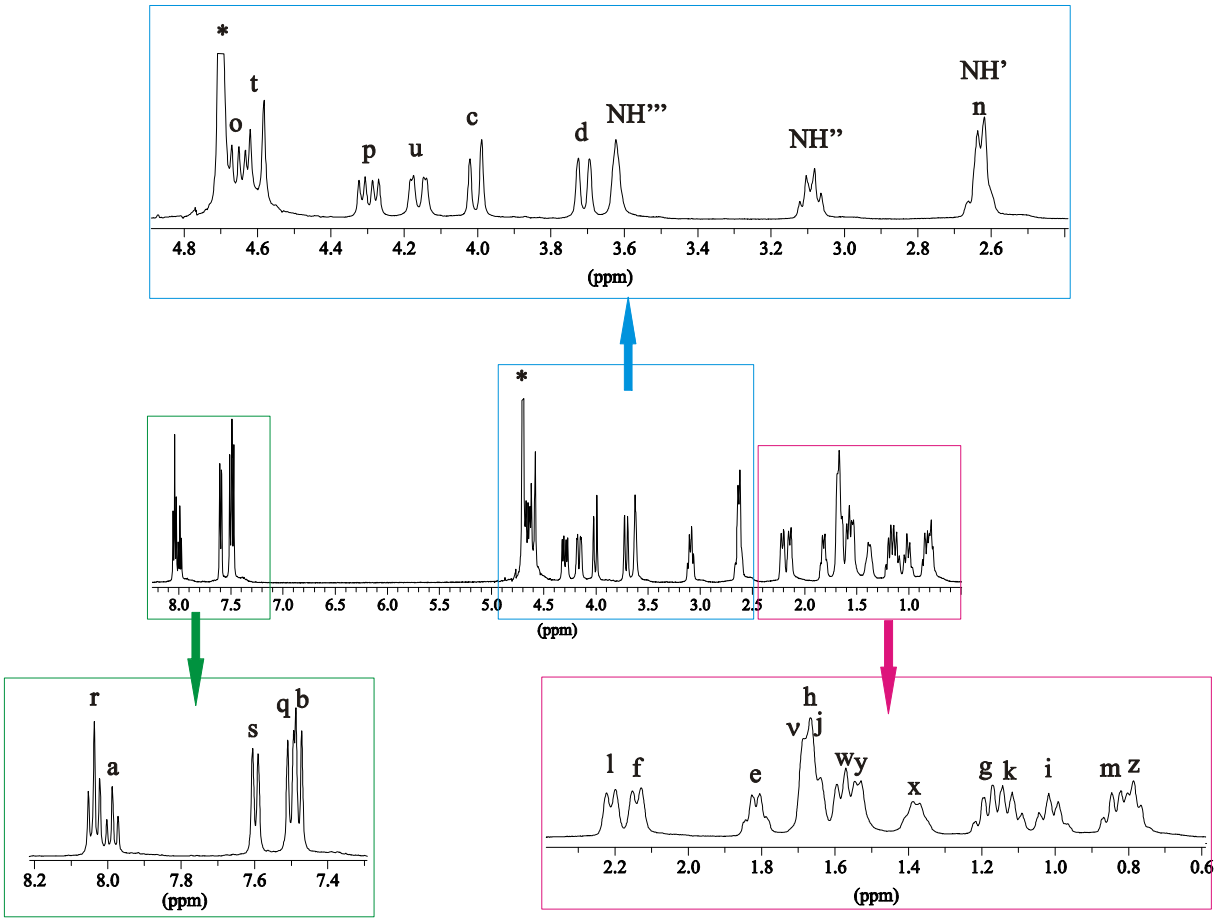

Fig. S25. The assignment of the signals in the ^{1}H NMR spectrum of the (*P*)-[Lu**L**$_{RRRRRR}$](NO$_3$)$_3$•7H$_2$O complex in D$_2$O solution (1 × 10^{-2} M, 298 K)

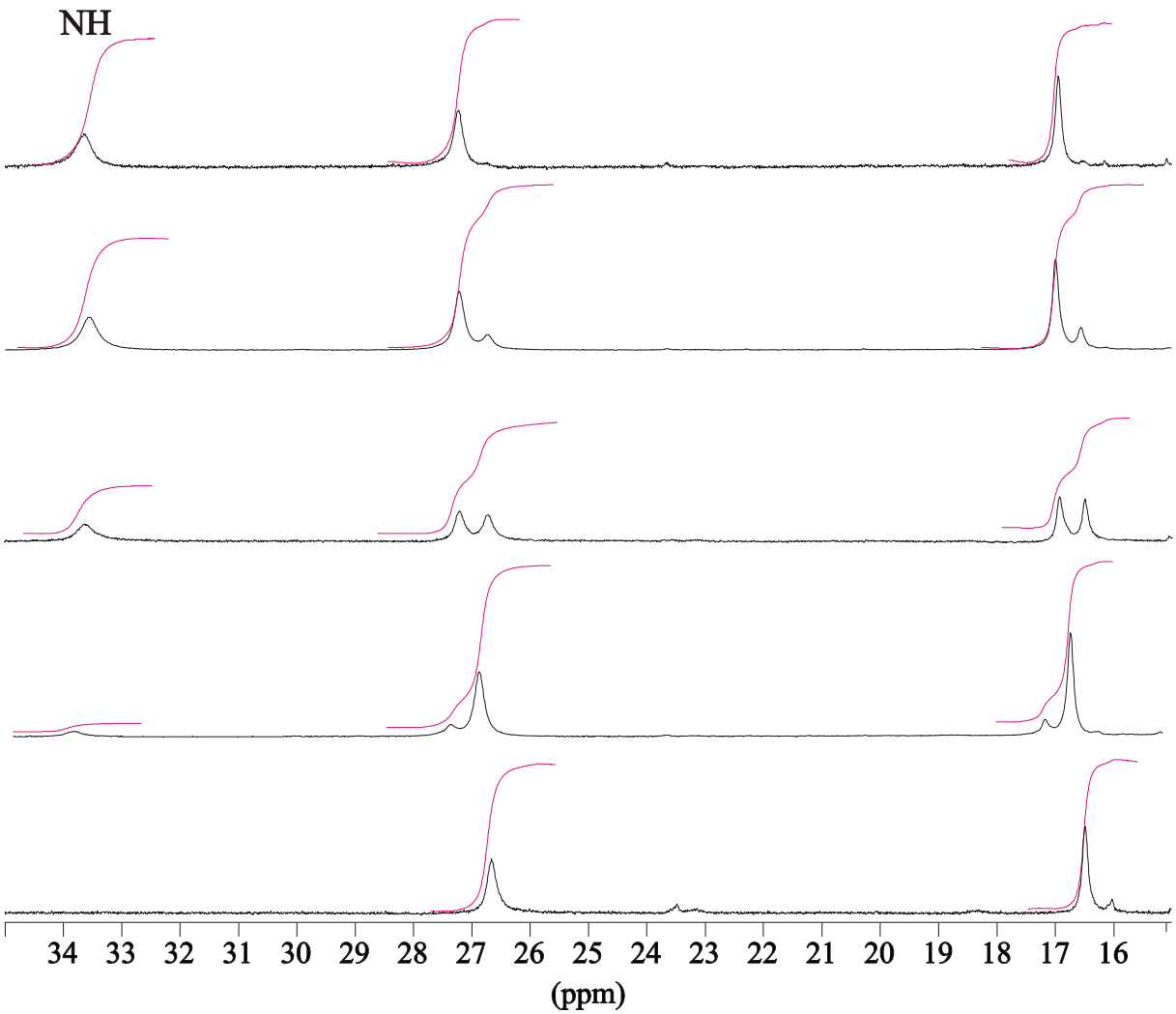

Fig. **S26**. The expanded region of Fig. S20; the ^{1}H NMR spectra of the (*M*)-[Yb**L** $_{RRRRRR}$](NO$_3$)$_3$]•CHCl$_3$•H$_2$O complex in CD$_3$OD solution (298 K), illustrating the doubling of the resonances due to isotope effect. The spectra were measured after 10 min (top), 1 hr, 3 hrs, 8 hrs and 22 hrs after preparation of the sample. The small signals in the bottom spectrum are due to the (*P*)-diastereomer formed in the helicity inversion process.

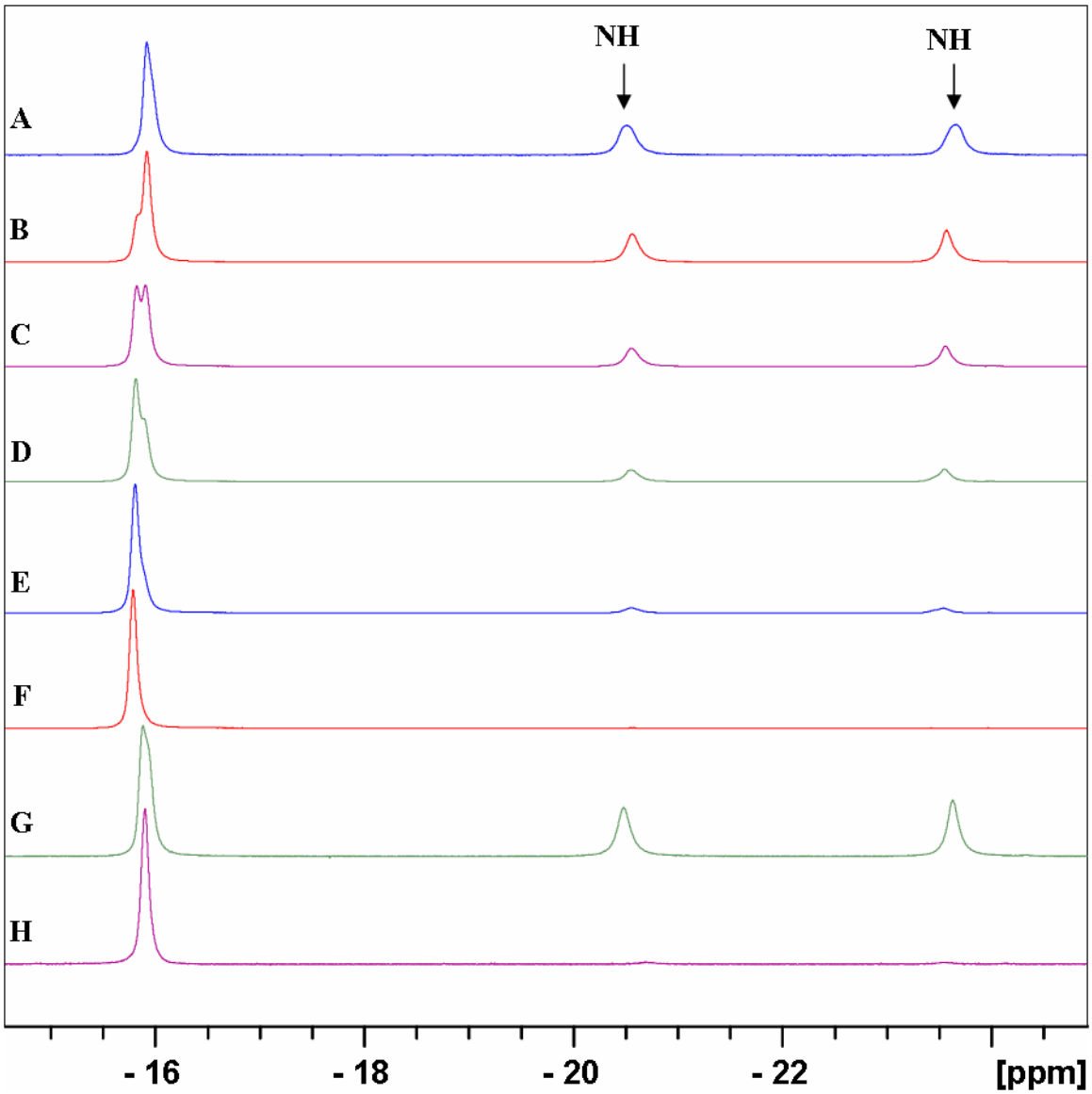

Supporting Fig. S27. The fragments of the ^{1}H NMR spectra (298K, CD_3OD) of *(M)*-[**PrL**$_{RRRRRR}$]$(NO_3)_3$•H_2O complex, illustrating the disappearing of NH signal and the influence of added acid/base. A – F : spectra measured after 0.16 h, 0.8 h, 1.8 h, 2.8h, 4.8h and 13h, respectively; G spectrum of a sample containing 10 μL of 6% HNO_3 measured after 4 h; G spectrum of a sample containing 5 μL of $N(C_2H_5)_3$ measured after 0.66 h.

Luminescence sensitization determination

The luminescence sensitization (η_{sens}) value was determined for the Eu(III) complex using the following equation[1]:

$$Q_{tot}^{Eu} = \eta_{ISC} \cdot \eta_{ET} \cdot Q^{Eu} = \eta_{sens} \cdot Q^{Eu}$$

where Q^{Eu}_{tot} is the europium-centred luminescence quantum yield obtained upon ligand excitation (0.03%), Q^{Eu} the intrinsic luminescence quantum yield of the Eu(III) ion, η_{sens} the efficiency of the luminescence sensitization by the ligand, η_{ISC} the efficiency of the intersystem crossing process from the ligand singlet to triplet state, and η_{ET} the efficiency of the ligand-to-metal energy transfer. The intrinsic quantum yield Q^{Eu} is defined as the ratio between the observed and radiative lifetimes of the Eu($^5D_0$) level:

$$Q^{Eu} = \tau_{obs}/\tau_R$$

where the radiative lifetime τ_R can be estimated from:

$$\tau_R = \frac{1}{A_{MD,0} \cdot n^3} \cdot \left(\frac{I_{MD}}{I_{tot}} \right)$$

$A_{MD,0}$ is the spontaneous emission probability of the Eu($^5D_0 \rightarrow {}^7F_1$) transition (14.65 s^{-1}), n is the refractive index (1.33 for the MeOH solution) and I_{MD}/I_{tot} is the intensity ratio of the Eu($^5D_0 \rightarrow {}^7F_1$) transition to the total emission of the $^5D_0$ level. For the Eu(III) complex with $\mathbf{L}_{\boldsymbol{RRRRRR}}$, I_{MD}/I_{tot} = 0.14, leading to τ_R = 4.1 ms, Q^{Eu} = 0.044 (τ_{obs} = 0.18 ms) and $\eta_{sens} = 7 \times 10^{-3}$. As a comparison, η_{sens} values of 0.03 (Q^{Eu}_L = 1.4%), 7×10^{-4} (Q^{Eu}_L = 0.01%), and in the range of 0.01-0.02 (Q^{Eu}_L ~1%) have been obtained for Eu(III) 1:1 and 1:2 complexes with the chiral ligand 2,6-bis(1-*S*-neopentylbenzimidazol-2-yl)pyridine,[2] and for Eu(III) 1:1 complexes with nitrobenzoic acid ligand derivatives,[3] respectively.

References

(1) Wertz, M. H. V.; Jukes, R. T. F.; Verhoeven, J. W. *Phys. Chem*. **1985**, *89*, 5649-5654

(2) Muller, G.; Maupin, C. L.; Riehl, J. P.; Birkedal, H.; Piguet, C.; Bunzli, J.-C. G. *Eur. J. Inorg. Chem.,* **2003**, 4065-4072

(3) de Bettencourt-Dias, A; Viswanathan, S. *Dalton Trans*, **2006**, 4093-4103.

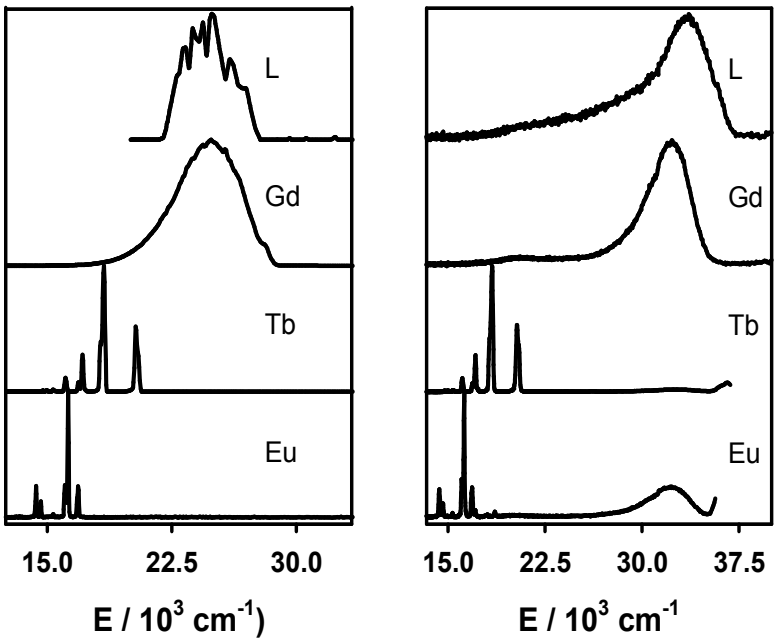

Figure S28. Left: Time-resolved emission spectra of $\mathbf{L}_{RRRRRR}$ and its Ln(III)-containing complexes in frozen MeOH solutions at 77 K and recorded with time delays of 0.1 or 0.5 ms. Right: Emission spectra of $\mathbf{L}_{RRRRRR}$ and its Ln(III)-containing complexes in MeOH solutions at 295 K (2-3 × 10^{-5} M and 3-4 × 10^{-4} M, respectively).

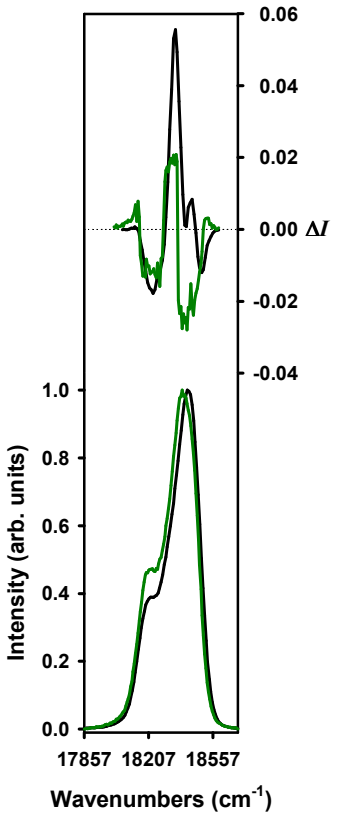

Figure S29. Circularly polarized luminescence (upper curve) and total luminescence (lower curve) spectra in the spectral range of the $^5D_4 \rightarrow {}^7F_5$ transition of (*M*)-[Tb$\mathbf{L}_{RRRRRR}$]$^{3+}$ measured before (black) and after (green) this 1×10^{-2} M complex solution in MeOH was heated at 328 K for three weeks, upon excitation at 284 nm, respectively.

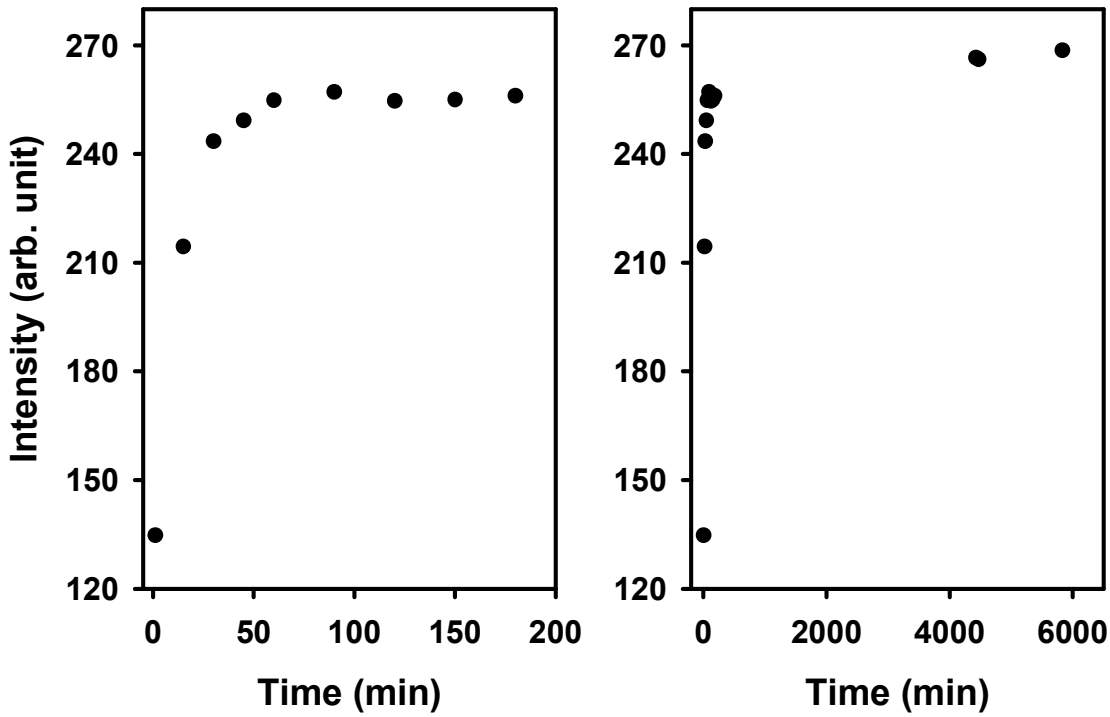

Fig. **S30**. Time dependence of the time-resolved emission intensities of the Eu(III)-containing complex with $\mathbf{L}_{RRRRRR}$ in 3×10^{-4} M CD_3OD solution at 295 K. The luminescence intensity has been monitored at 615 nm for 200 (left) and 6000 minutes (right).

Kinetic analysis

The k_1 rate of conversion of the (*M*)-[Ln**L**$_{RRRRRR}$]$^{3+}$ diasteromer to the (*P*)-[Ln**L**$_{RRRRRR}$]$^{3+}$ diastereomer:

$$(M)LnL \underset{k2}{\overset{k1}{\rightleftarrows}} (P)LnL$$

was estimated on the basis of the equations:

$$\ln\left(\frac{[(M)LnL]_0 - [(M)LnL]_{eq}}{[(M)LnL]_t - [(M)LnL]_{eq}}\right) = (k_1 + k_1)t \quad \text{and} \quad K_{eq} = \frac{[(P)LnL]_{eq}}{[(M)LnL]_{eq}} = \frac{k_1}{k_2}$$

The sum of k_1 and k_2 was obtained from the plots of the negative natural logarithm of the concentration of (M)-diastereomer in time minus the equilibrium concentration of this diastereomer versus time. For the (*M*)-[Lu**L**$_{RRRRRR}$](NO$_3$)$_3$•CHCl$_3$•2H$_2$O complex the conversion to the (P)-diastereomer is practically complete and the rate constant was based on an approximation of the first-order reaction. The partial decomposition of the complexes to the free ligand was not taken into account in the kinetic analysis. The analysis yielded the rough estimation of k_1 rate constants to be equal to 1x10^{-6} s^{-1}, 1.4x10^{-6} s^{-1}, 6.5x10^{-6} s^{-1} and 3.1x10^{-6} s^{-1} for the Tb, Er, Yb and Lu complexes, respectively.

The first-order rates of H/D exchange corresponding to the reaction :

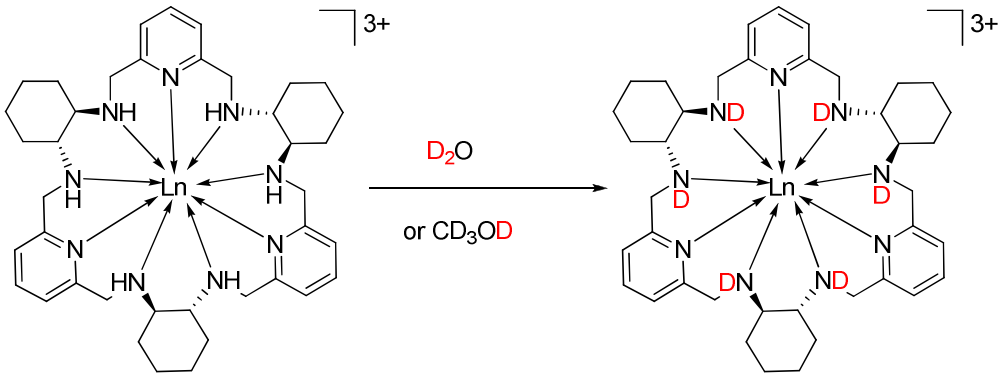

was calculated by analyzing the plots of natural logarithm of the intensity of the NH signals vs. time.

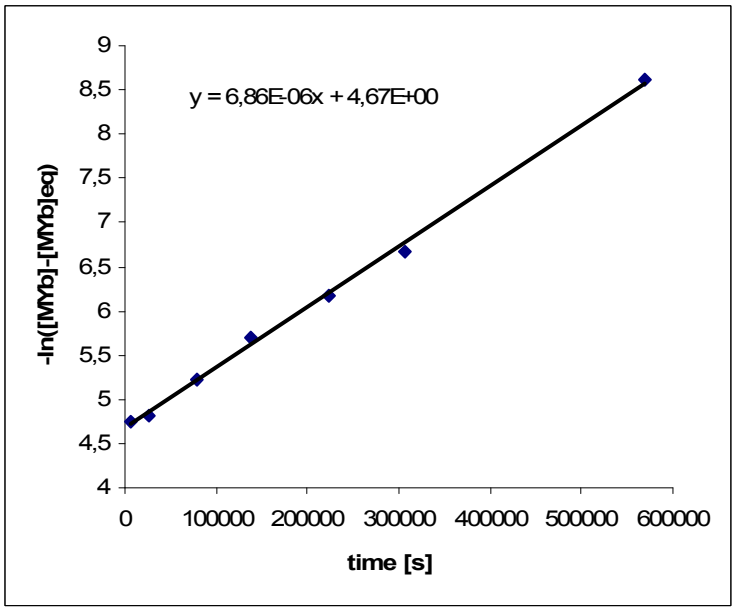

Fig. S31. The plot of the negative natural logarithm of the concentration of (M)-diastereomer in time minus the equilibrium concentration of this diastereomer versus time for the (M)-[Yb$\mathbf{L}_{RRRRRR}$]$(NO_3)_3$]•$CHCl_3$•H_2O complex (D_2O, 318 K).

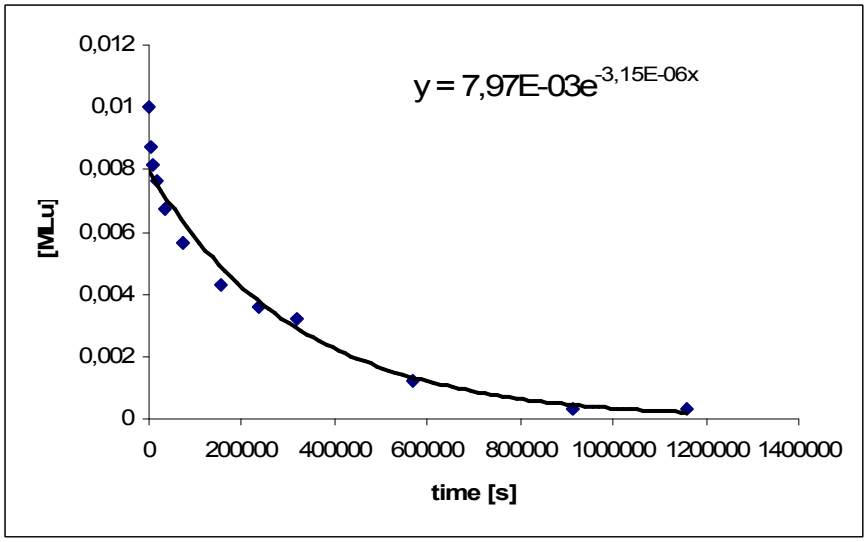

Fig. S32. The plot of the concentration of (M)-diastereomer vs. time for the (*M*)-[Lu$\mathbf{L}_{RRRRRR}$]$(NO_3)_3$•$CHCl_3$•$2H_2O$ complex (D_2O, 318 K).

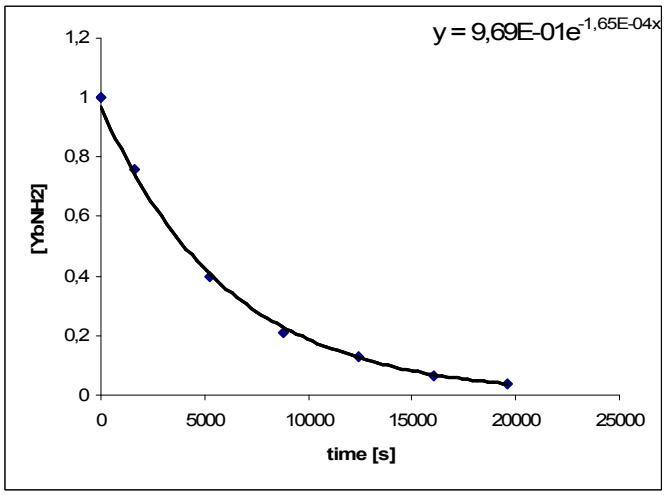

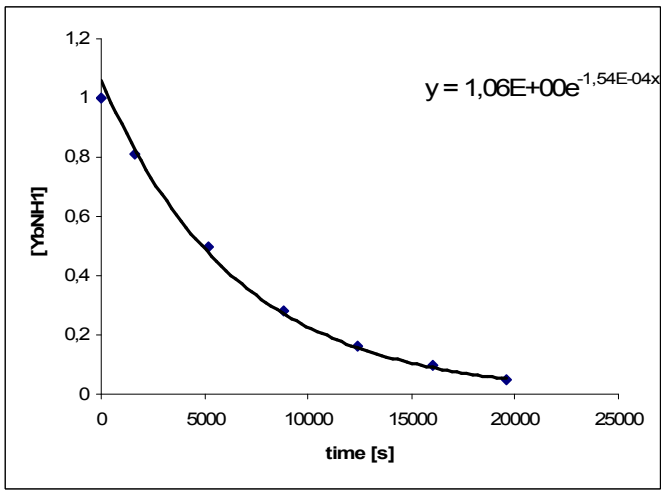

Fig. S33. The plots of the concentrations of the NH signals (based on the ^{1}H NMR signal intensity) vs. time for the two different amine protons of the (*P*)-[Yb**L**$_{RRRRRR}$](NO$_3$)$_3$•6H$_2$O complex (298K, CD$_3$OD).

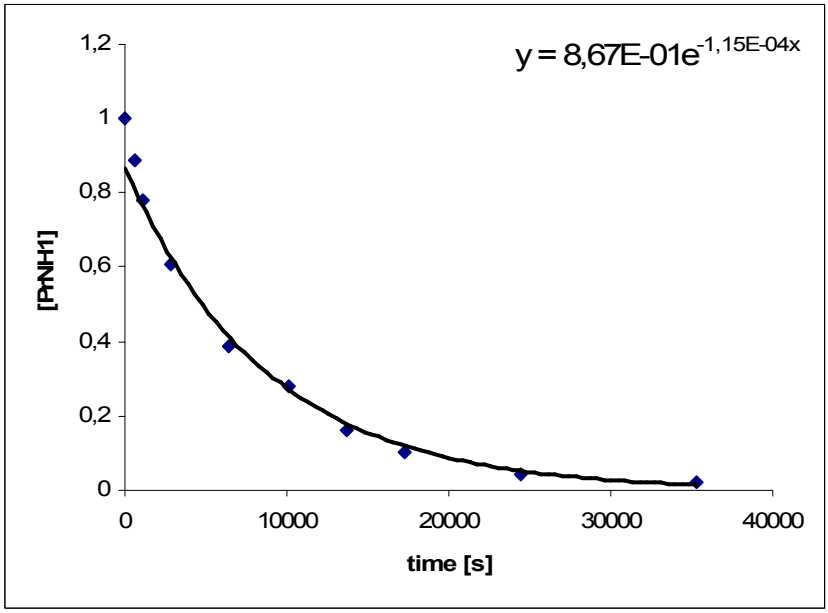

Fig. S34. The plot of the concentration of the NH signal (based on the ^{1}H NMR signal intensity) vs. time for the amine proton of the *(M)*-[Pr**L**$_{RRRRRR}$](NO$_3$)$_3$•H$_2$O complex (298K, CD$_3$OD).

Supporting Table S1

Crystal data and structure refinement details for the (*M*)-[PrL_{RRRRRR}]$(NO_3)_3$•3CH_3CN•$3^2/_3H_2O$, (*P*)-[CeL_{SSSSSS}]$(NO_3)_3$•4CH_3CN•3H_2O and (*P*)-[LuL_{RRRRRR}]$(NO_3)_3$•$1^7/_8CH_3CN$•$3^3/_4H_2O$ complexes.

Empirical formula	$C_{45}H_{73.33}N_{15}O_{12.67}Pr$	$C_{47}H_{75}CeN_{16}O_{12}$	$C_{42.75}H_{70.13}LuN_{13.88}O_{12.75}$
Formula weight	1168.11	1196.35	1157.47
Temperature	100(2) K	100(2) K	100(2) K
Wavelength	0.71073 Å	0.71073 Å	0.71073 Å
Crystal system	orthorhombic	orthorhombic	trigonal
Space group	$P2_12_12_1$	$P2_12_12_1$	$P322_1$
Unit cell dimensions	a = 13.486(8) Å	a = 13.469(3) Å	a = 14.982(4) Å
	b = 14.542(8) Å	b = 14.537(3) Å	c = 38.92(2) Å
	c = 28.702(17) Å	c = 28.830(6) Å	
Volume	5629(6) $Å^3$	5645(2) $Å^3$	7566(5) $Å^3$
Z	4	4	6
Density (calculated)	1.380 g/cm^3	1.408 g/cm^3	1.524 g/cm^3
Absorption coefficient	0.936 mm^{-1}	0.878 mm^{-1}	2.032 mm^{-1}
F(000)	2437	2492	3581
Crystal size	0.462×0.281×0.163 mm	0.30×0.20×0.15 mm	0.4×0.15×0.1 mm
ϑ range for data collection	3.1 to 36.7°	2.60 to 28.72°	3.0 to 28.6°
Index ranges	-22≤h≤17,	-17≤h≤18,	-19≤h≤19,
	-13≤k≤19,	-19≤k≤19,	-19≤k≤20,
	-38≤l≤38	-38≤l≤29	-52≤l≤33
Reflections collected	42480	40745	50951
Independent reflections	14547 (Rint = 0.0613)	13646 (Rint = 0.0499)	12056 (Rint = 0.0602)
Absorption correction	analytical	analytical	analytical
Max. and min. transmission	0.875 and 0.751	0.893 and 0.808	0.793 and 0.537
Refinement method	full-matrix least-squares on F2	full-matrix least-squares on F2	full-matrix least-squares on F2
Data/restraints/parameters	14547/0/669	13646/6/683	12056/6/629
Goodness-of-fit on F^2	1.037	1.077	0.991
Final R indices [I>2σ(I)]	R(F) = 0.0590	R(F) = 0.0502	R(F) = 0.0413
	$R_w(F^2)$ = 0.1333	$R_w(F^2)$ = 0.1145	$R_w(F^2)$ = 0.0715
R indices (all data)	R(F) = 0.0815,	R(F) = 0.0678	R(F) = 0.0647
	$R_w(F^2)$ = 0.1408	$R_w(F^2)$ = 0.1225	$R_w(F^2)$ = 0.0748
Absolute structure parameter	0.027(15)	0.012(14)	-0.020(7)
Largest diff. peak and hole	1.814 and -1.689 e.$Å^{-3}$	1.687 and -0.895 e.$Å^{-3}$	1.818 and -0.600 e.$Å^{-3}$

Supporting Table S2. Selected bond lengths (Å) for $[PrL_{RRRRRR}](NO_3)_3 \bullet 3CH_3CN \bullet 3^2/_3H_2O$, (*P*)-$[CeL_{SSSSSS}](NO_3)_3 \bullet 4CH_3CN \bullet 3H_2O$ and $[LuL_{RRRRRR}](NO_3)_3 \bullet 1^7/_8\ CH_3CN \bullet 3^3/_4H_2O$ crystals.

Empirical formula	$C_{45}H_{73.33}N_{15}O_{12.67}Pr$	$C_{47}H_{75}CeN_{16}O_{12}$	$C_{42.75}H_{70.13}LuN_{13.88}O_{12.75}$
Ln-N1	2.600(6)	2.620(4)	2.493(4)
Ln-N2	2.698(5)	2.708(4)	2.559(4)
Ln-N3	2.652(5)	2.663(4)	2.534(4)
Ln-N4	2.624(4)	2.645(4)	2.451(4)
Ln-N5	2.701(5)	2.714(4)	2.532(4)
Ln-N6	2.683(6)	2.697(4)	2.525(4)
Ln-N7	2.633(5)	2.649(4)	2.447(4)
Ln-N8	2.637(5)	2.657(4)	2.526(4)
Ln-N9	2.719(5)	2.723(4)	2.577(4)

Supporting Table S3. Final distribution of species obtained after heating the solutions of the (*M*)-$[Ln\mathbf{L}_{RRRRRR}]^{3+}$complexes in D_2O at 318K.

Ln	Total time of heating [hrs]	%*(M)*-$[Ln\mathbf{L}_{RRRRRR}]^{3+}$	%*(P)*-$[Ln\mathbf{L}_{RRRRRR}]^{3+}$	%$\mathbf{L}_{RRRRRR}$
Ce	87	1	0	99
Pr	1375	89.5	0	10.5
Eu	1393	78.1	17.2	4.7
Tb	1395	52.9	42.3	4.7
Er	1394	11	89	a
Yb	326	5	88.8	6.2
Lu	894	1.1	80	18.9

[a] could not be determined due to signal broadening